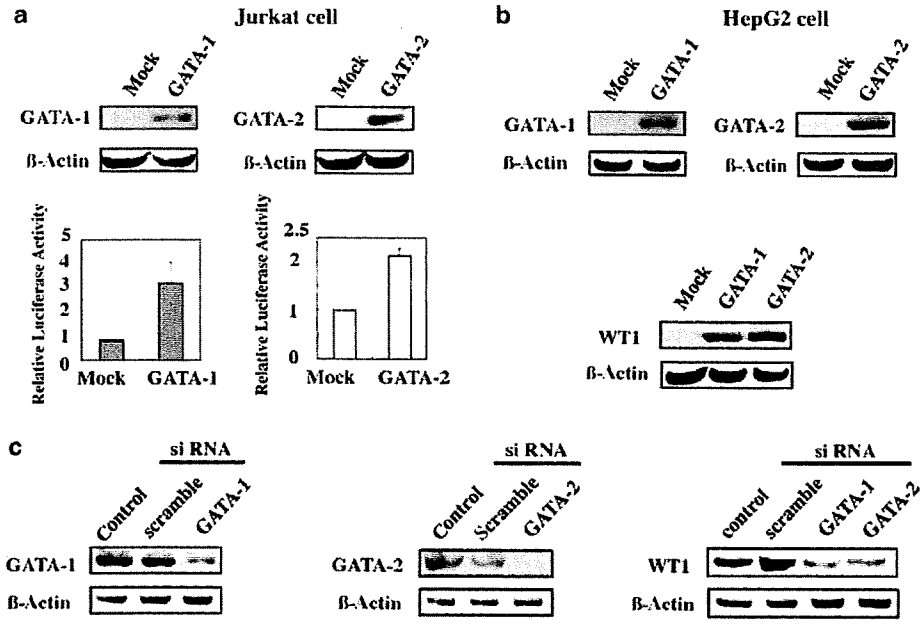


**Figure 5** Effect of modulation of GATA family genes. *GATA-1* and *GATA-2* expression vectors were transiently introduced to Jurkat and HepG2 cells whose original *WT1* mRNA levels were low. Under overexpression conditions shown in the upper parts of **a** and **b**, we determined *WT1* promoter/enhancer activities using the e2 reporter of Figure 4c (**a**), or WT1 protein levels (**b**). Promoter/enhancer activity was expressed with the mock transfectant regarded as 1.0. (**c**) siRNAs of GATA-1 and GATA-2 were transfected as described in the Materials and methods. At 48 h after transfection, the WT1 protein level was evaluated by western blotting with β-actin as the internal control ( right). Scramble siRNA was used as the control of the specificity of siRNAs used.

cells was only faintly detectable, probably because of the low transfection efficiency (data not shown). However, increased *WT1* promoter activity of Jurkat cells by transient *GATA-1* and *GATA-2* expression was clearly observed (Figure 5a). siRNA of *GATA-1* and *GATA-2* effectively inhibits WT1 expression (Figure 5c). Our quantitative reverse transcriptase-PCR, western blotting and promoter/enhancer analyses, and siRNA analysis showed that not only *GATA-1* but also *GATA-2* mRNA was expressed in both leukemia cell lines and clinical samples, and that GATA-1 and GATA-2 are equally effective in *WT1* gene expression by binding to a GATA site located in the 3'-enhancer region.

### *EMSA analysis of the distal GATA site of 3' enhancer*

In EMSA, using the two most distal GATA sites (Figure 6a upper), several retarded bands (a, b, c and d) were observed in K562 nuclear extract, with smaller amounts in Jurkat and Daudi cells (Figure 6a lower). The intensities of the retarded bands were in proportion to their *WT1* mRNA levels (Figure 2). The cold competitor erased all the retarded bands supporting their specificity (Figure 6b left). The probe with a mutated distal GATA site (mut2), which is the same as m3 in Figure 4c, produced no retarded bands other than band d, suggesting that a, b and c bands are produced by GATA binding to the distal site (Figure 6c left); another probe with the mutated proximal GATA site (mut1) (described as m2 in Figure 4c) produced band patterns similar to those of wild-type probe (wt), supporting the results of our promoter analysis (Figure 4). Both anti-GATA-1 and anti-GATA-2 antibody to K562 nuclear extract inhibited bands a, b and c, suggesting that both GATA-1 and GATA-2 were the factors bound to this GATA site (Figure 6d upper).

We also examined solid tumors, TYK-nu-cPr and several other cell lines. EMSA of TYK-nu-cPr differed from those of k562 cells (Figure 6a lower-right). In addition to the commonly observed band d, we also observed bands e and f. They are also competed with the cold competitor (Figure 6b right). Interestingly, the band pattern of HL60 with GATA-2, but not GATA-1 expression, was similar to that of TYK-n-cPr (Figure 6a). The probe with the mutated GATA site (mut1), but not mut2, produced band e, which was reduced by anti-GATA-2 but not anti-GATA-1 antibody (Figures 6c and d).

The molecular weight and function of GATA-1 and GATA-2 were not markedly different. The difference observed in the EMSA pattern between K562 and TYK-nu-cPr was unexpected and quite interesting. Treatment with anti-GATA-1 and anti-GATA-2 antibodies showed that both GATA-1 and GATA-2 bound to the same GATA motif, and that GATA-2, but not GATA-1, was bound in TYK-nu-cPr cells. The complex formation between the GATA family and other cofactors might explain the different patterns observed. Further analysis is needed to elucidate the real binding mode of these GATA factors.

### *Chromatin immunoprecipitation assay using anti-GATA-1 and anti-GATA-2 antibodies*

To confirm our EMSA data, a chromatin immunoprecipitation assay was carried out. Figure 7 shows that both GATA-1 and GATA-2 bound the 3' enhancer sequence in K562 cells, and that GATA-2, but not GATA-1, bound this enhancer in TYK-nu-cPr cells, a finding consistent with our promoter/enhancer analysis and EMSA data.

## Conclusion

Taken together, these results showed that not only GATA-1[14,15] but also GATA-2 bound to the most distal GATA site of

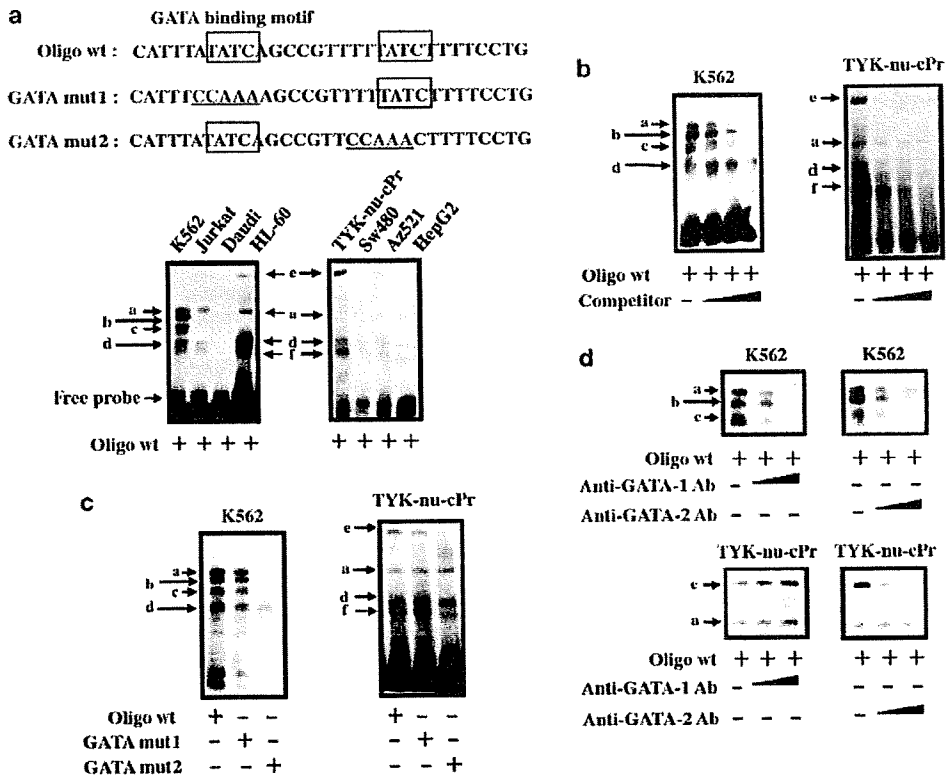


**Figure 6** (**a**) EMSA analysis using probes covering the two distal GATA sites. Using biotin-labeled probes containing the two most distal GATA sites (oligo wild type, GATA mut1 and GATA mut2), the binding of transcription factor was examined using nuclear extracts from K562, Jurkat, Daudi, or HL60 cells (left) and TYk-nu-cPr, SW480, Az521 or HepG2 cells (right). Retarded bands were named a, b, c, d, e and f, respectively. (**b**) In addition to the labeled probe, a cold probe (x1–x10 excess) was added to the reaction mixture of K562 and TYK-nu-cPr cells, and EMSA was carried out. (**c**) A labeled probe with wild-type or with the mutated GATA site (GATA mut1 or GATA mut2 shown in (**a**) was used. (**d**) Anti-GATA-1 (final concentration: from 0.1 to 10 μg/ml) or anti-GATA-2 (final concentration: from 0.1 to 10 μg/ml) was added to nuclear extracts before incubation with the labeled DNA probe, as described in Materials and methods.

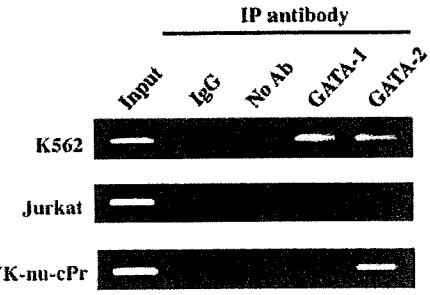


**Figure 7** Chromatin immunoprecipitation assay was carried out as described in Materials and methods. After immunoprecipitation with anti-GATA-1 or anti-GATA-2 antibody, DNA was purified. PCR was performed using a primer set covering the region 123 bp long containing the two most distal GATA sites (Materials and methods). For specificity control, samples treated with unrelated IgG or PBS (no Ab) are also shown.

3' enhancer, which was the important determinant of the *WT1* mRNA level in some cell lines. Furthermore, this 3' enhancer is not unique to a hematopoietic lineage but has also proven effective in solid tumor cell lines. The regulatory mechanism of *WT1* gene expression described in these experiments provides the fundamental information on the WT1 biology of malignant diseases.

## Acknowledgements

We express our sincere thanks to Dr H Nagai and Ms K Hagiwara (National Hospital Organization, Nagoya Medical Center, Nagoya, Japan) and to Dr Y Oji and Dr H Sugiyama (Osaka University Graduate School of Medicine, Osaka, Japan) for providing us with cell lines and useful comments. We acknowledge Ms Y Nomura for her excellent cell-sorting work. This work was supported in part by a Grant-in-Aid for Basic Research C 16590453 and by Health and Labour Research Grants from the Ministry of Health, Labour and Welfare, Japan.

## References

1 Hewitt SM, Hamada S, McDonnell TJ, Rauscher III FJ, Saunder GF. Regulation of the proto-oncogenes bcl-2 and c-myc by the Wilms' tumor suppressor gene, *WT1*. *Cancer Res* 1995; **55**: 5386–5389.
2 Lou XN, Reddy JC, Yeyeti PL, Idris AH, Hosono S, Haber DA *et al*. The tumor suppressor gene *WT1* inhibits ras-mediated transformation. *Oncogene* 1995; **11**: 743–750.
3 Keilholz U, Menssen HD, Gaiger A, Menke A, Oji Y, Oka J *et al*. Wilms' tumour gene 1 (*WT1*) in human neoplasia. *Leukemia* 2005; **19**: 13181–13323.
4 Haber DA, Sohn RL, Buckler AJ, Pelletier J, Call KM, Housman DE. Alternative splicing and genomic structure of the Wilms tumor gene *WT1*. *Proc Natl Acad Sci USA* 1991; **88**: 9618–9622.

5 Loeb DM. WT1 influences apoptosis through transcriptional regulation of Bcl-2 family members. *Cell Cycle* 2006; **5**: 1249–1253.
6 Jomgeow T, Oji Y, Tsuji N, Ikeda Y, Ito K, Tsuda A *et al.* Wilms' tumor gene *WT1* 17AA(−)/KTS(−) isoform induces morphological changes and promotes cell migration and invasion *in vitro*. *Cancer Sci* 2006; **97**: 259–270.
7 Ito K, Oji Y, Tatsumi N, Shimizu S, Kanai Y, Nakazawa T *et al.* Antiapoptotic function of 17AA(+) *WT1* (Wilms' tumor gene) isoforms on the intrinsic apoptosis pathway. *Oncogene* 2006; **25**: 4217–4229.
8 Oji Y, Ogawa H, Tamaki H, Oka Y, Tsuboi A, Kim EM *et al.* Expression of the Wilms' tumor gene *WT1* in solid tumors and its involvement in tumor cell growth. *Int J Cancer Res* 1999; **90**: 194–204.
9 Boublikova L, Kalinova M, Ryan J, Quinn F, O'Marcaigh A, Smith O *et al.* Wilms' tumor gene 1 (*WT1*) expression in childhood acute lymphoblastic leukemia: a wide range of WT1 expression levels, its impact on prognosis and minimal residual disease monitoring. *Leukemia* 2006; **20**: 254–263.
10 Tamaki H, Ogawa H, Ohyashiki K, Ohyashiki JH, Iwama H, Inoue K *et al.* The Wilms' tumor gene *WT1* is a good marker for diagnosis of disease progression of myelodysplastic syndromes. *Leukemia* 1999; **13**: 393–399.
11 Weisser M, Kern W, Rauhut S, Schoch C, Hiddemann W, Haferlach T *et al.* Prognostic impact of RT-PCR-based quantification of *WT1* gene expression during MRD monitoring of acute myeloid leukemia. *Leukemia* 2005; **19**: 1416–1423.
12 Yang L, Han Y, Suarez Saiz F, Minden MD. A tumor suppressor and oncogene: the WT1 story. *Leukemia* 2007; **21**: 868–876.
13 Cohen HT, Bossone SA, Zhu G, McDonald GA, Sukhatme VP. Sp1 is a critical regulator of the Wilms' tumor-1 gene. *J Biol Chem* 1997; **272**: 2901–2913.
14 Fraizer GC, Wu YJ, Hewitt SM, Maity T, Yon CC, Huff V *et al.* Transcriptional regulation of the human Wilms' tumor gene (*WT1*): cell type-specific enhancer and promiscuous promoter. *J Biol Chem* 1994; **269**: 8892–8900.
15 Wu Y, Fraizer GC, Saunders GF. GATA-1 transactivates the WT1 hematopoietic specific enhancer. *J Biol Chem* 1995; **270**: 5944–5949.
16 Hosen N, Yanagihara M, Nakazawa T, Kanato K, Nishida S, Asada T *et al.* Identification of a gene element essential for leukemia-specific expression of transgenes. *Leukemia* 2004; **18**: 415–419.
17 Dehbi M, Pelletier J. PAX-8-mediated activation of the *wt1* tumor suppressor gene. *EMBO J* 1996; **15**: 4297–4306.
18 Siehl JM, Thiel E, Heufelder K, Snarski E, Schwartz S, Mailander V *et al.* Possible regulation of Wilms' tumour gene 1 (*WT1*) expression by the paired box genes PAX2 and PAX8 and by the haematopoietic transcription factor GATA-1 in human acute myeloid leukaemias. *Br J Haematol* 2003; **123**: 235–242.
19 Fraizer GC, Shimamura R, Zhang X, Saunders GF. PAX 8 regulates human WT1 transcription through a novel DNA binding site. *J Biol Chem* 1997; **272**: 30678–30687.
20 Zhang X, Xing G, Fraizer GC, Saunders F. Transactivation of an intronic hematopoietic-specific enhancer of the human Wilms' tumor 1 gene by GATA-1 and c-Myb. *J Biol Chem* 1997; **272**: 29272–29280.
21 Ohneda K, Yamamoto M. Roles of hematopoietic transcription factors GATA-1 and GATA-2 in the development of red blood cell lineage. *Acta Hematol* 2002; **108**: 237–245.
22 Weiss MJ, Orkin SH. GATA transcription factors: key regulators of hematopoiesis. *Exp Hematol* 1995; **23**: 99–107.
23 Shimamoto T, Ohyashiki K, Ohyashiki JH, Kawakubo K, Fujimura T, Iwama H *et al.* The expression pattern of erythrocyte/megakaryocyte-related transcription factor GATA-1 and the stem cell leukemia gene correlates with hematopoietic differentiation and is associated with outcome of acute myeloid leukemia. *Blood* 1995; **86**: 3173–3180.
24 Iwasaki T, Sugisaki C, Nagata K, Takagi A, Kojima T, Ito M *et al.* Wilms' tumor 1 message and protein expression in bone marrow failure syndrome and acute leukemia. *Pathol Int* 2007; **57**: 645–651.
25 Sobue S, Iwasaki T, Sugisaki S, Nagata K, Kikuchi R, Murakami M *et al.* Quantitative RT-PCR analysis of sphingolipid metabolic enzymes in acute leukemia and myelodysplastic syndromes. *Leukemia* 2006; **20**: 2042–2046.
26 Kikuchi R, Murakami M, Sobue S, Iwasaki T, Hagiwara K, Takagi A *et al.* Ewing's sarcoma fusion protein, EWS/Fli-1 and Fli-1 protein induce PLD2 but not PLD1 gene expression by binding to an ETS domain of 5′ promoter. *Oncogene* 2007; **26**: 1802–1810.
27 Ho IC, Vorhees P, Marin N, Oakley BK, Tsai SF, Orkin SH *et al.* Human GATA-3: a lineage-restricted transcription factor that regulates the expression of the T cell receptor alpha gene. *EMBO J* 1991; **10**: 1187–1192.
28 Ko L, Yamamoto M, Leonard MW, George KM, Ting P, Engel JD. Murine and human T-lymphocyte GATA-3 factors mediate transcription through a cis-regulatory element within the human T-cell receptor delta gene enhancer. *Mol Cell Biol* 1991; **11**: 2778–2784.
29 Tagge EP, Hanson P, Re GG, Othersen Jr HB, Smith CD, Garvin AJ. Paired box gene expression in Wilms' tumor. *J Pediatr Surg* 1994; **29**: 134–141.
30 Dressler GR, Douglas EC. Pax-2 is a DNA-binding protein expressed in embryonic kidney and Wilms tumor. *Proc Natl Acad Sci USA* 1992; **89**: 1179–1183.
31 Hosen N, Sonoda Y, Oji Y, Kimura T, Minamiguchi H, Tamaki H *et al.* Very low frequencies of human normal CD34+ haematopoietic progenitor cells express the Wilms' tumor gene WT1 at levels similar to those in leukemia cells. *Br J Haematol* 2002; **116**: 409–420.
32 Mouthon MA, Bernard O, Mitjavila MT, Romeo PH, Vainshenker W, Mathieu-Mahul D. Expression of tal-1 and GATA-binding proteins during human hematopoiesis. *Blood* 1993; **81**: 647–655.
33 Maratheftis CI, Bolaraki PE, Voulgarelis M. GATA-1 transcription factor is up-regulated in bone marrow hematopoietic progenitor CD34(+) and erythroid CD71(+) cells in myelodysplastic syndromes. *Am J Hematol* 2007; **82**: 887–892.

Supplementary information accompanies the paper on the Leukemia website (http://www.nature.com/leu)

# The oral iron chelator deferasirox represses signaling through the mTOR in myeloid leukemia cells by enhancing expression of REDD1

Junko H. Ohyashiki,[1,3] Chiaki Kobayashi,[2] Ryoko Hamamura,[2] Seiichi Okabe,[2] Tetsuzo Tauchi[2] and Kazuma Ohyashiki[2]

[1]Intractable Diseases Therapeutic Research Center, Tokyo Medical University, Tokyo 160-0023; [2]First Department of Internal Medicine, Tokyo Medical University, Tokyo 160-0023, Japan

(Received December 11, 2008/Revised January 21, 2009/Accepted January 22, 2009/Online publication March 9, 2009)

**To evaluate the effect of deferasirox in human myeloid leukemia cells, and to identify the molecular pathways responsible for antiproliferative effects on leukemia cells during chelation therapy, we performed gene expression profiling to focus on the pathway involved in the anticancer effect of deferasirox. The inhibitory concentration ($IC_{50}$) of deferasirox was 17–50 μM in three human myeloid cell lines (K562, U937, and HL60), while those in fresh leukemia cells obtained from four patients it varied from 88 to 172 μM. Gene expression profiling using Affymerix GeneChips (U133 Plus 2.0) revealed up-regulation of cyclin-dependent kinase inhibitor 1A (*CDKN1A*) encoding $p21^{CIP}$, genes regulating interferon (i.e. *IFIT1*). Pathways related to iron metabolism and hypoxia such as growth differentiation factor 15 (*GDF-15*) and Regulated in development and DNA damage response (*REDD1*) were also prominent. Based on the results obtained from gene expression profiling, we particularly focused on the REDD1/mTOR (mammalian target of rapamycin) pathway in deferasirox-treated K562 cells, and found an enhanced expression of REDD1 and its down-stream protein, tuberin (TSC2). Notably, S6 ribosomal protein as well as phosphorylated S6, which is known to be a target of mTOR, was significantly repressed in deferasirox-treated K562 cells, and REDD1 small interfering RNA restored phosphorylation of S6. Although iron chelation may affect multiple signaling pathways related to cell survival, our data support the conclusion that REDD1 functions up-stream of tuberin to down-regulate the mTOR pathway in response to deferasirox. Deferasirox might not only have benefit for iron chelation but also may be an antiproliferative agent in some myeloid leukemias, especially patients who need both iron chelation and reduction of leukemia cells. (*Cancer Sci* 2009; 100: 970–977)**

Iron plays a central role in the regulation of many cellular functions.[1] Evidence suggests that iron is required for cell survival and proliferation, and perturbation in cellular iron uptake can arrest cell growth both *in vitro* and *in vivo*.[2] As a part of ribonucleotide reductase, the enzyme responsible for deoxyribonucleotides synthesis, iron is an essential growth factor and rate-limiting trace element in DNA synthesis.[3] Dysregulaton of iron metabolism leads to iron overloading associated with deleterious effects on cells and tissues.[3] Numerous iron chelators have been synthesized in order to treat iron overload diseases, especially thalassemia. Evidence suggests the hyperproliferative effect of iron overload in a subset of cancer cells and iron depletion by chelators inhibits the proliferation of cancer cells, including leukemia cells.[4–8] Among the different molecules synthesized, hexadenate deferoxamine (DFO) is the major molecule used for the treatment of iron overload. However, it is highly hydrophilic, and inactive if taken perorally. For this reason, the perorally active iron chelator, deferasirox, is of special interest, since recent reports demonstrated that it acts as a potent nuclear factor kappa-light-chain-enhancer of activated B cell (NF-kappa-B) inhibitor and improves hematological data in a subset of patients with myelodysplastic syndromes (MDS).[9,10]

To evaluate the effect of deferasirox (also knows as ICL670, Novartis, Basel, Switzerland), and to identify molecular pathways responsible for the observed reduced transfusion requirement during chelation therapy, we performed gene expression profiling to focus on the pathway involved in the anticancer effect of deferasirox.

## Materials and Methods

**Reagents and cell cultures.** The oral iron chelator, deferasirox was donated by Novartis. We purchased three human myeloid leukemia cell lines, K562, U937, and HL-60 from Health Science Research Resources Bank (Osaka, Japan) for this study. Cells were grown in RPMI1640 with 10% fetal bovine serum. After obtaining written informed consent, peripheral blood mononuclear cells (PBMCs) were isolated from four patients with acute myeloid leukemia (AML) by the Ficoll-Hypaque technique. This study was approved by our institutional medical ethics committee.

**Cell viability and apoptosis assay.** The inhibitory effect of deferasirox on cell growth was assessed by a Cell Counting Kit-8 (Wako Chemicals, Tokyo, Japan). Briefly, the cells (5000 cells/well) were incubated in triplicate in a 96-well plate in the presence or absence of indicated test samples at a final volume of 0.1 mL for 48 h at 37°C. Thereafter, 0.01 mL of tetrazolium salt, WST-1, was added to each well. After 2-h incubation at 37°C, the optical density (OD) at 450 nm was measured using a 96-well multiscanner autoreader with the extraction buffer used as a blank. Cell viability was expressed as a percentage (OD of the experiment sample/OD of the control × 100). Inhibitory concentration ($IC_{50}$) was calculated by GraphPad Prism 5 (GraphPad Software, La Jolla, CA, USA). For detection of apoptosis, caspase-3/7 activity was analyzed by the Caspase-Glo 3/7 assay (Promega, Madison, WI, USA). This test provides a pro-luminescent caspase-3/7 substrate, which contains the caspase-specific tetrapeptide sequence DEVD in a reagent, and determination of caspase and luciferase activity. The addition of a caspase-3/7 reagent results in cell lysis, followed by caspase-mediated cleavage of the Z-DEVD, release of luciferase reaction and finally the generation of luminescence.[11]

**Gene expression and microarray data analysis.** K562 cells were exposed to 10 μM or 50 μM ($IC_{50}$ dose) of deferasirox for 24 h. After treatment, cells were harvested, and total RNA was extracted using an RNeasy Mini Kit (Qiagen, Germantown, MD, USA). The amount of RNA was measured by NanoDrop (NanoDrop Technologies, Wilmington, DE, USA), then the quality of extracted RNA was checked using a 2100 Bioanalyzer (Agilent Technologies, Wilmington, DE, USA). Gene expression profiling was done using the GeneChip U133 Plus 2.0 (Affymetrix, Santa Clara, CA, USA),

[3]To whom correspondence should be addressed. E-mail: junko@hh.iij4u.or.jp



doi: 10.1111/j.1349-7006.2009.01131.x

according to the manufacturer's instructions. Experiments were done in duplicate, and the microarray data were deposited in GEO (NCBI, Gene Expression Omnibus). For statistical analysis of gene expression, we utilized a GeneSifter® (geospiza, Seattle, WA, USA). Analysis of variance (ANOVA), and Student's *t*-test, were done using GeneSifter®. *P*-values of less than 0.05 were considered to indicate a statistically significant difference and the Benjamini-Hochberg algorithm was used for estimation of false discovery rates.[12]

**Real-time reverse transcriptase polymerase chain reaction (RT-PCR).** To confirm the microarray results, we performed RT-PCR by an ABI Prism 7700 Sequence Detection System (Applied Biosystems, Foster City, CA, USA) as we reported elsewhere.[13] We used Taqman gene expression assays for *REDD1* (Regulated in development and DNA damage response, assay ID: Hs00430304_gl; Applied Biosystems), and the amount of gene expression in each sample was evaluated as a percent of the standard curve generated from a serial dilution of quantitative PCR human reference total RNA (Stratagene, La Jolla, CA, USA). The obtained data from glyceraldehyde 3-phosphate dehydrogenase (*GAPDH*) were used to standardize the sample variation in the amount of input cDNA.

**Immunoblotting.** Cells were cultured for 24 h following respective treatments. Cells were washed twice in ice-cold phosphate-buffered saline (PBS) and cell pellets were lyzed in buffer containing 50 mM Tris-HCl (pH 7.5), 150 mM NaCl, 1% NP-40, 0.5% sodium dodecylsulfate (SDS) and a cocktail of protease inhibitors (Roche Diagnostics, Mannheim, Germany) at 4°C for 20 min. After centrifugation at 10000*g* for 20 min at 4°C, equal amounts of proteins were resolved by SDS-polyacrylamide gel electrophoresis (SDS-PAGE). The separated proteins were blotted onto a polyvinylidene difluoride (PDVF) membrane (Bio-Rad, Hercules, CA, USA). After blockage of non-specific binding sites with BlockAce (Dainippon-Sumitomo Pharma, Osaka, Japan), the filter was incubated with the following antibodies for 60 min at room temperature; REDD1 (Protein Tech Group, Inc., Chicago, IL, USA), tuberin (Santa Cruz Biotechnology, Santa Cruz, CA, USA), mammalian target of rapamycin (mTOR) (Cell Signaling, Denver, MA, USA), phosphorylated mTOR (S2448) (Cell Signaling), p70S6 kinase (Cell Signaling), phosphorylated S6 (Cell Signaling), and antiactin (Chemicon International Inc., Temecula, CA, USA). After washing, the blots were incubated for 60 min with horseradish peroxidase (HRP)-linked antimouse or antirabbit IgG (GE Healthcare, Buckinghamshire, UK). Signals were visualized using ECL Western blotting detection reagents and analysis system (GE Healthcare).

**Small interfering RNA (siRNA).** siRNA oligonucleotides for the REDD1 and GAPDH (control) were purchased from Thermo Scientific Dharmacon (Waltham, MA, USA) and resuspended in RNase-free-$H_2O$ according to the manufacturer's instructions. K562 cells were transfected with REDD1 or control siRNA in the presence or absence of 50 μM of deferasirox. For cell transfection, approximately $1 \times 10^6$ cells were plated in 96-well plates to give 50% confluency. The cells were transfected with siRNA using a Gene Pulser electroporation system, then 48 h after transfection with REDD1 or control siRNA, deferasirox or dimethyl sulfoxide (DMSO) were added to the culture. The efficacy of transfection was evaluated by Western blotting as well as real-time RT-PCR as we reported elsewhere.[14]

**Action of deferasirox in nude mice bearing transplantable human myelogenous leukemic cell line.** For the *in vivo* assessment of deferasirox, 6-week-old female nude mice were injected with U937 cells and then assigned randomly to either the distilled water alone or deferasirox treatment groups. At 24 h after the injection, these mice were orally given either distilled water or deferasirox (50 mg/kg, daily) dissolved in distilled water. Mice were observed daily, and their body weight as well as signs of stress (e.g. lethargy, ruffled coat, or ataxia) were used to detect possible toxicities. The average tumor weight per mouse was calculated and used to analyze the group mean tumor weight ± SE ($n = 10$ mice). Tumors were collected at the predetermined times and fixed in paraformaldehyde.

**Table 1. Inhibitory concentration of ICL670 (deferasirox) in human myeloid leukemia cells**

| Cells | | Deferasirox (μM) |
|---|---|---|
| Cell lines | K562 | 46.33 |
| | U937 | 16.91 |
| | HL-60 | 50 |
| Patient specimen | UPN1: post-MDS-AML | 87.63 |
| | UPN2: AML (M0) | 92.17 |
| | UPN3: AML(M4) | 89.65 |
| | UPN4: refractory AML (M5) | 172.2 |

MDS, myelodysplastic syndromes; AML, acute myeloid leukemia.

Paraffin-embedded tissues were sectioned and processed for gross histopathology by hematoxylin–eosin staining or by the terminal deoxynuceotidyl transferase-mediated dUTP-biotin nick-end labeling (TUNEL) method to evaluate apoptosis.[15]

## Results

**Deferasirox-induced cell death in myeloid leukemia cells.** We first examined the effects of deferasirox *in vitro* in various myeloid leukemia cells by a cell-counting assay. The median inhibitory concentration ($IC_{50}$) of deferasirox for K562 cells was 46.33 μM, that for U937 was 16.91 μM, that for HL-60 was 50 μM, respectively, and those for fresh leukemia cells obtained from four AML patients ranged from 87.63 to 172.2 μM (Table 1). To determine whether or not the cell death induced by deferasirox was due to apoptosis in myeloid leukemia cell lines, K562, U937, and HL60, we measured the activity of caspase-3/7 by a Caspase-Glo 3/7 kit (Promega). The number of viable cells were counted after 24 h exposure to deferasirox, in order to normalize the caspase-3/7 activity with respect to the number of cells per well. In all three leukemia cell lines tested, the activity of caspase-3/7 significantly increased after 50 μM deferasirox exposure (Fig. 1A–C). As shown in Fig. 1(D), the fold increase of apoptosis after normalization of cell numbers was evident in a dose-dependent manner.

**Gene expression profile of deferasirox-treated K562 cells.** To further understand how deferasirox induced cell death in human myeloid cells, K562 cells were treated with deferasirox or control for short time-periods, and microarray analysis was performed using a GeneChip (GEO, GPL570). Differential expression was analyzed using a GeneSifter®. All the microarray data was deposited in GEO (GSE11670: http://www.ncbi.nlm.nih.gov/geo/query/acc.cgi?token=fparzqkgqugqexi&acc=GSE11670). Up-regulated or down-regulated genes in deferasirox-treated K562 cells (expression level in the sample was 4-fold greater or lower than in untreated cells) are listed in Table 2. The salient features of up-regulated genes are summarized as follows. First, up-regulation of genes related to cell-cycle regulation was evident; cyclin G2 and cyclin-dependent kinase inhibitor 1A (*CDKN1A*) encoding p21, CDK-interacting protein1 (Cip). Second, genes regulating interferon were also up-regulated: interferon-induced protein with teteratricopeptide repeat 1 (*IFIT1*, *ISG56*), *IFIT3* (*ISG 60*), and interleukin 23 A (*IL23A*), which stimulate the production of interferon-γ. Third, genes related to apoptosis, such as *inhibin-β*, *B-cell lymphoma* (*BCL6*), pleckstrin homolog-like domain family A member 1 (*PHLDA1*), Bcl2/adenovirus E1B19-kDa protein-interacting protein 3-like (*BNIP3L*), tribbles homolog 3 (*TRIB2*), a negative regulator of NF-κB, were up-regulated. Fourth, growth differentiation factor 15 (*GDF15*), which is currently known as a negative regulator of the iron regulatory protein hepcidin, is remarkably up-regulated. Finally, it is notable that genes closely related to the oxygen regulatory system, including those regulated in development and DNA damage responses 1 (*REDD1*, also known as a HIF-1 responsive protein, RTP801), and phosphoglycerate

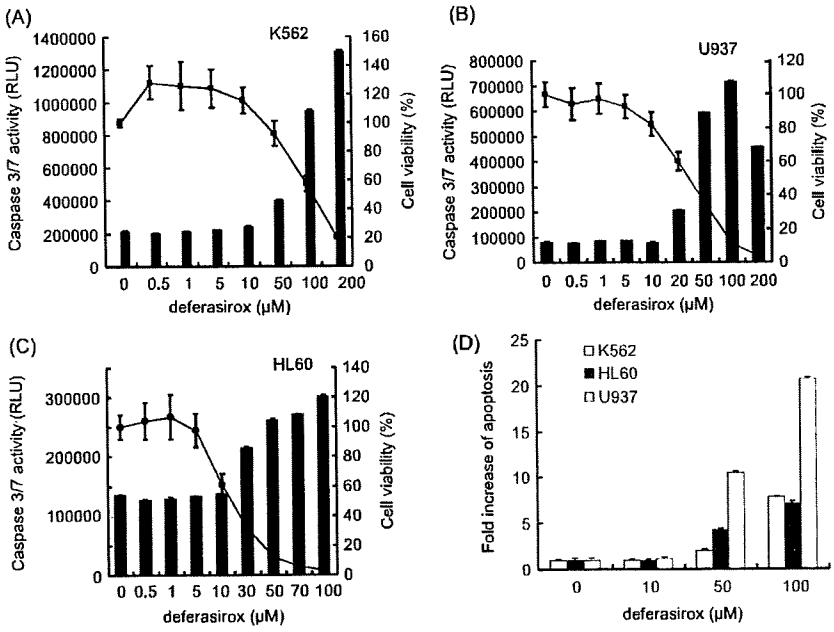


**Fig. 1.** Deferasirox-induced cell death in myeloid leukemia cell lines (A, K562; B, U937; C, HL60). Left *Y* axis indicates caspase 3/7 activity in $IC_{50}$ dose of deferasiox-treated cell lines. The 'no cell' blank control value was subtracted from each reading. The percentage of viability is plotted with respect to untreated cells (right *Y* axis). The results are shown as means (±SD) percentage of viability from triplicate cultures with repeated experiments. (D) Caspase-3/7 activity is expressed relative to untreated control cells.

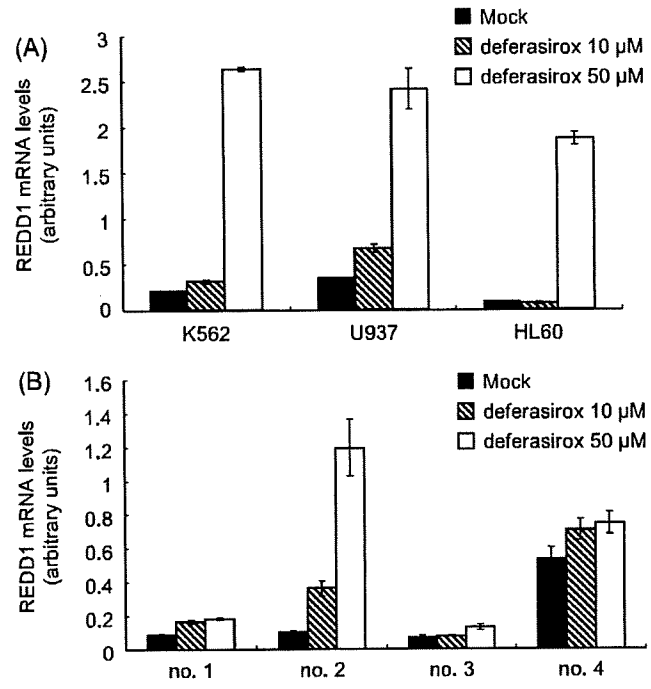


**Fig. 2.** Up-regulation of Regulated in development and DNA damage response (REDD1) expression in human myeloid leukemia cells. Relative REDD1 messenger RNA (mRNA) levels are determined using real time reverse transcription – polymerase chain reaction. The REDD1 gene expression level is normalized to the *GAPDH* mRNA levels as reported previously (Ref. no. 13). (A) The REDD1 gene expression is remarkably up-regulated in human myeloid leukemia cell lines. (B) REDD1 gene expression in fresh leukemia cells obtained from four patients.

dehydrogenase (*PHGDH*), which is related to NO metabolism, are up-regulated. Unlike up-regulated genes, we could not subdivide the extracted genes according to the molecular function; however, we found down-regulation of solute carrier family 5 member 6 (*SLC5A6*), which is related to iron-transport.

**Up-regulation of *REDD1* in deferasirox-treated myeloid leukemia cells.** Based on the results obtained from the differential expression pattern, we particularly focused our study on a gene closely related to oxygen regulation, *REDD1*. To determine whether up-regulation of *REDD1* takes place ubiquitously in the antitumor activity of deferasirox, we examined the change of *REDD1* expression by real-time RT-PCR in three human myeloid leukemia cell lines. Cells were treated with or without deferasirox (10 μM and 50 μM) for 24 h, and total RNA was collected. The *REDD1* expression remarkably increased after deferasirox treatment with a more than 2-fold increase of *REDD1* expression at 50 μM deferasirox, in all three leukemia cell lines (Fig. 2A). We also examined *REDD1* expression in four samples obtained from AML patients. Although the degree of increased *REDD1* expression varies among the samples, *REDD1* expression was up-regulated after deferasirox treatment in some freshly obtained samples from AML patients (Fig. 2B).

**REDD1 suppresses S6 ribosomal protein via mTOR pathways.** We therefore focused on the REDD1/TSC (tuberous sclerosis complex) pathway, which modulate mTOR signaling. An important mechanism through which mTOR signaling is regulated involves the Tuberin-Hamartin complex. We found up-regulation of TSC2 (tuberin) in accordance with REDD1 in deferasirox-treated K562 cells (Fig. 3A). Since TSC1 is regulated by V-AKT murine thymoma viral oncogene homolog 1 (AKT), we also examined the AKT expression in deferasirox-treated K562 cells. However, AKT protein expression was not altered after deferasirox treatment (data not shown). This indicates that TSC2 is up-regulated through the REDD1/TSC2 pathway, rather than the AKT/TSC2 pathway. Subsequently, phosphorylated mTOR, and phosphrylated-p70S6kinase, decreased in a dose-dependent manner (Fig. 3A,B). We noted a dose-dependent decrease of phophorylated-S6 protein, which is known as a downstream effecter of mTOR, in K562 cells treated with 50 μM of deferasirox (Fig. 3A bottom), indicating that deferasirox inhibits ribosomal S6 via mTOR pathway in K562 cells. Down-regulation of phosphorylated ribosomal S6 protein was also found in deferasirox-treated U937 and HL60 cells (Supporting File S1).

**Inhibition of REDD1 resutores S6 ribosomal protein.** To assess whether or not the enhanced expression of REDD1 mRNA was necessary for repression of mTOR signaling, siRNAs direct against the human REDD1 mRNA were used to reduce its expression in K562 cells in the presence or absence of deferasirox. Treatment



doi: 10.1111/j.1349-7006.2009.01131.x

**Table 2. Genes altered in deferasirox-treated K562 cells**

| No. | Gene ID | Gene name | Molecular function | *P*-value |
|---|---|---|---|---|
| I. Up-regulated genes in deferasirox-treated K562 cells | | | | |
| 1 | INHBE | Inhibin beta E | Hormone activity | 0.00051 |
| 2 | IFIT1 | Interferon-induced protein with tetratricopeptide repeats 1, ISG56 | Immune response | 0.000906 |
| 3 | MYEF2 | Myeloin expression factor 2 | Transcription | 0.000224 |
| 4 | REDD1 | Regulated in development and DNA damage responsed 1,DNA damage-inducible transcript 4, DDIT4, HIF1-responsive protein RTP801 | Inhibitor of mtor pathway | 0.000027 |
| 5 | PHGDH | Phosphoglycerate dehydrogenase | L-serine biosynthetic process; regulation of oxideructase activity (Redox) | 0.000002 |
| 6 | ATF3 | Activating transcription factor 3 | Regulation of transcription, DNA-dependent | 0.000016 |
| 7 | TP53INP1 | P53-dependent damage-inducible nuclear protein 1 | P53-dependent apoptosis | 0.001184 |
| 8 | ASNS | Asparagine synthetase | Asparagine biosynthetic process; NO metabolism | 0.000063 |
| 9 | GDF15 | Growth differentiation factor 15 | Signal transduction; TGF beta family | 0.000003 |
| 10 | IL8 | Interleukin 8 | Angiogenesis | 0.000298 |
| 11 | CTH | Cystathionase (cystathionine gamma-lyase) | Amino acid biosynthetic process | 0.000034 |
| 12 | MYO5A | Myosin VA (heavy polypeptide 12, myoxin) | Transport | 0.000445 |
| 13 | GADD153 | DNA-damage-inducible transcript 3, DDIT3 | Cell cycle arrest | 0.000344 |
| 14 | MAPKAPK5 | Mitogen-activated protein kinase-activated protein kinase 5 | Protein amino acid phosphorylation | 0.000489 |
| 15 | BCL6 | B-cell CLL lymphoma 6 | Protein import into nucleus, translocation | 0.000156 |
| 16 | PMAIP1 | Phorbol-12-myristate-13-acetate-induced protein 1 | Release of cytochrome c from mitochondria | 0.000019 |
| 17 | CCNG2 | Cyclin G2 | Regulation of progression through cell cycle | 0.000653 |
| 18 | HPSE | Heparanase precursor | Proteoglycan metabolic process | 0.000714 |
| 19 | CDKN1A | Cyclin-dependent kinase inhibitor 1 A (p21, Cip1) | Response to DNA damage stimulus | 0.000104 |
| 21 | PHLDA1 | Pleckstrin homology-like domain, family A, member 1 | Apoptosis | 0.000129 |
| 22 | BNIP3L | Bcl2/adenovirus E1B 19-kdprotein-interacting protein 3-like | Apoptosis | 0.000146 |
| 23 | NR4A1 | Nuclear receptor subfamily 4, group A, member 1 | Transcription: MAPK signaling | 0.000739 |
| 24 | IFIT3 | Interferon-induced protein with tetratricopeptide repeats 3, ISG 60 | Immune response | 0.000355 |
| 25 | IL23A | Interleukin 23-alpha | Inflammatory response; stimulate the production of interferon-gamma (ifng) | 0.000503 |
| 26 | IGF1 | Insulin-like growth factor 1 (somatomedin C) | Skeletal development | 0.000059 |
| 27 | TRIB3 | Tribbles homolog 3 (Drosophila) | Negative regulator of NF-kappaB | 0.000409 |
| II. Down-regulated genes in ICL670 treated K562 cells | | | | |
| 28 | TNFSF13B | Tumor necrosis factor ligand superfamily, member 13 | B cell homeostasis | 0.001076 |
| 29 | LYAR | cDNA DKFZp434G0514 | Protein binding | 0.000295 |
| 30 | SLC5A6 | Solute carrier family 5 (sodium-dependent vitamin transporter), member 6 (SLC5A6) | Ion transport | 0.000018 |
| 31 | PCDH12 | Protocadherin 12 | Cell adhesion | 0.000589 |
| 32 | EVI1 | Ecotropic viral integration site 1 | Multicellular organismal development | 0.001132 |
| 33 | FABP5 | Fatty acid binding protein 5 (psoriasis-associated) | Lipid metabolic process | 0.000627 |
| 34 | RLBP1 | Retinaldehyde-binding protein 1 | Vitamin a metabolic process | 0.000011 |
| 35 | DRD1 | D-1 dopamine receptor | Signal transduction | 0.000388 |
| 36 | CDH7 | Cadherin 7 | Homophilic cell adhesion | 0.000282 |
| 37 | CCDC14 | cDNA clone ZE16C03 | Electron transport | 0.000862 |
| 38 | CCDC39 | cDNA DKFZp434A128 | Mitochondrion | 0.000062 |

of REDD1 siRNA caused a reduction in REDD1 expression to ~50% of the value observed in untreated cells or cells that had been treated with control siRNA (Fig. 4A). Moreover, treatment of REDD1 siRNA prior to deferasirox dramatically attenuated the drug-induced expression of REDD1 (Fig. 4B). Notably, deferasirox-induced decrease in S6K1 phosphorylation was blocked by REDD1 siRNA treatment. In contrast, the control siRNA had no effect on the deferasirox-induced decrease in S6K1 phosphorylation.

**Deferasirox supresses heterotransplated tumor growth in nude mice bearing myeloid leukemia cells.** To further study the activity of deferasirox on tumor growth *in vivo*, we tested a mouse model of human myeloid leukemia. Subcutaneous injection of U937 cells into nude mice resulted in an aggressive malignancy resembling acute leukemia, characterized by tumor, splenomegaly, and invasion of leukemia cells into hematopoietic and non-hematopoietic tissue: some of them had ascites without obvious tumor formation at the injected area. The control mice (distilled water alone) died of a condition resembling acute leukemia or tumor-bearing by 50 days; however, 2/10 mice treated with deferasirox survived for more than 90 days; deferasirox-treated mice tended to survive longer than those with saline ($P = 0.2450$) (Fig. 5A). The tumor volume of the subcutaneous tumors was significantly smaller in mice treated by deferasirox compared to those with vehicle alone ($P < 0.0001$) (Fig. 5B). No deferasirox-treated mice showed any adverse events. Histopathological analysis of xenotransplant mice revealed infiltration of the spleen and bone marrow with leukemic blasts. In contrast, deferasirox-treated mice demonstrated distinct morphological changes, including condensed nucleoli and an increasing number of apoptotic cells detected by the TUNEL method (Fig. 5C). These results indicate that deferasirox yields a desirable therapeutic index that can reduce the *in vivo* growth of myeloid leukemia cells in an efficacious manner.

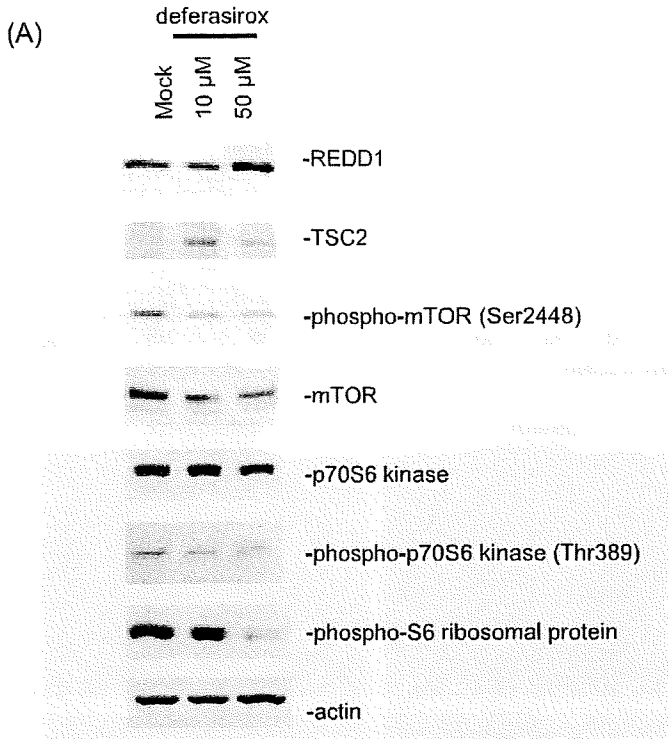


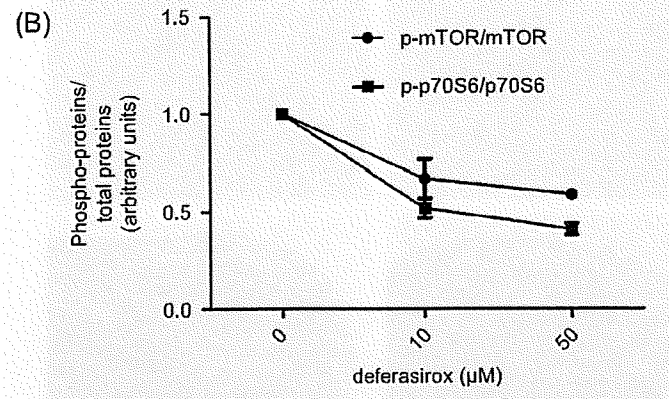


**Fig. 3.** Western blot analysis of K562 cells with or without treatment by deferasirox (10 μM and 50 μM). (A) Expression of Regulated in development and DNA damage response (REDD1) and tuberous sclerosis complex 2 (TSC2) are increased in deferasirox-treated K562 cells. Phosphorylated mammalian target of rapamycin (mTOR), phosphorylated-p70S6 kinase and phosphorylated S6 ribosomal protein, were decreased in a dose-dependent manner. (B) The intensity of signals were measured by a Versa-Doc gel imaging system (Bio-Rad Laboratories, Hercules, CA, USA). The ratio of phophorylated protein per total protein is expressed as an arbitrary unit. We confirmed the dose-dependent decrease of phosphorylated mTOR and phophorylated-p70S6 proteins in deferasirox-treated K562 cells.

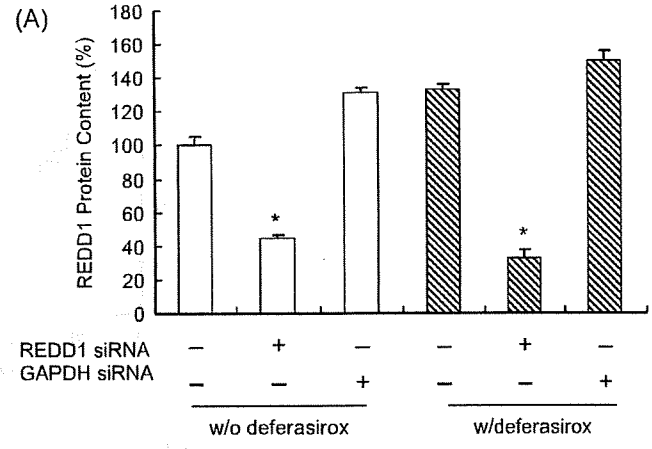


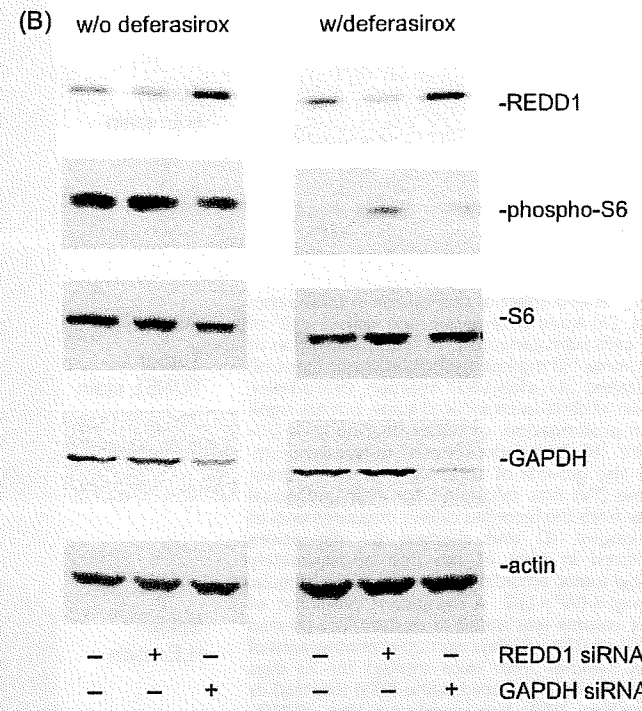


**Fig. 4.** Inhibition of Regulated in development and DNA damage response (REDD1) by small interfering RNA (siRNA) in the presence or absence of deferasirox in K562 cells. (A) REDD1 siRNA induced phosphorylation of S6 ribosomal protein in cells with or without deferasirox. However, the effect was more evident in deferasirox-treated K562 cells. (B) REDD1 protein contents are expressed as a percent with respect to untreated cells. Administration of REDD1 siRNA caused a reduction in REDD1 expression up to 50% of the value observed in untreated cells or cells that had been administrated a control glyceraldehyde 3-phosphate dehydrogenase (GAPDH) siRNA.

## Discussion

We set out to determine the moleclular pathways responsible for antiproliferative effects on human myeloid leukemia cells during chelation therapy. The antiproliferative effect of iron chelating agents has been well recognized.[4,7,16–18] However, in the past, the exact mechanism of the antineoplastic effects of iron chelator were not clearly determined. Among iron chelators, deferasirox has been shown to have higher antiproliferative effects by apoptosis in cultured human hepatocytes and hepatocellular carcinoma cell lines than O-trensox,[19,20] and deferasirox is now available as an oral iron chelator. Chantrel-Graussard *et al.* further demonstrated that deferasirox induced cell cycle blockade in the G2-M phase and inhibited polyamine biosynthesis by decreasing ornithine decarboxylase and spermidine N1-acethyltransferase activities and decreasing ornithine decarboxylase mRNA level,[19] and they concluded that deferasirox has powerful antineoplastic effects and blocks cell proliferation in neoplastic cells by a pathway different from that of other iron chelators. However, they only refer to a limited number of reports regarding antiproliferative effect on human leukemia cells. Iron is critical for DNA synthesis and energy



doi: 10.1111/j.1349-7006.2009.01131.x

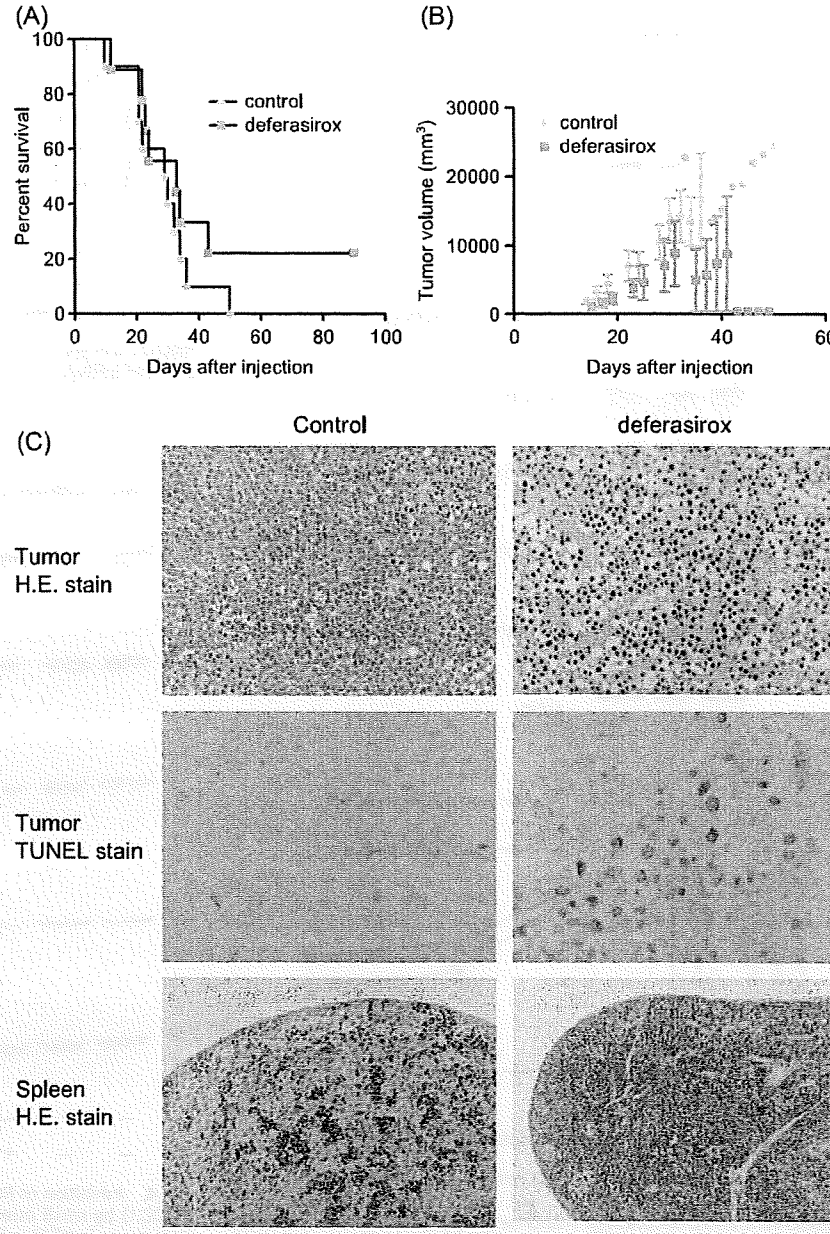


**Fig. 5.** *In vivo* effect of deferasirox in U937 xenografts. (A) Nude mice inoculated with $5 \times 10^6$ of U937 cells subcutaneously. Oral administration of deferasirox (50 mg/kg) or distilled water (control) was started 24 h after U937 injection. Oral administration of deferasirox induced some, but not significant, prolongation, of tumor-bearing mice ($P = 0.2450$). (B) Orally administered deferasirox inhibited the growth of U937 cells *in vivo*. Tumor volume (TV) was calculated for each individual mouse from the recorded caliper measurements of the longest (L) and shortest (L) dimensions (expressed in mm) of the one approximately ellipsoid tumor, according to the following formula: TV (mg) = $(W^2 \times L)/2$. A significant reduction of tumor volume was noted in desferasirox-treated mice ($P < 0.0001$). (c) Representative photographs of biopsy samples from mice treated for 23 days with phosphate buffered saline (PBS) (control) or deferasirox. H&E: hematoxyline-eosine; TUNEL, TdT-mediated dUTP nicked-end labeling. Original magnification ×200.

production, and neoplastic cells require more iron for their rapid proliferation.[2] Iron depletion inhibits iron-containing enzymes, ribonucleotide reductase, and up-regulates proapoptic proteins, Bax, caspase-3, caspase-8, and caspase-9 that induce apoptosis. Recently, orally available deferasirox has been given to patients with MDS to prevent excess iron deposition. Evidence suggests that iron chelation therapy actually reduces transfusion requirements, and improves some hematological findings in a subset of MDS patients, regardless of the percentage of blasts.[21] These findings lead us to consider molecular mechanisms of iron chelation by which proliferation of leukemic cells are inhibited.

In the current study, we demonstrated the cytotoxic effects due to apoptosis in human leukemia cell lines and freshly obtained leukemia cells from AML patients. The $IC_{50}$ value of these cells ranged from 17 μM to 50 μM in leukemia cell lines and 87 μM to 172 μM in fresh leukemia cells. Since the phase I study of deferasirox treatment for heavily transfused patients receiving daily oral deferasirox of 20 mg/kg (the recommended dose for iron chelation therapy) demonstrated that 100 μM could be achieved *in vivo*,[22] the pharmacological dose of the antiproliferative effect *in vitro* is considered to be reasonable.

Gene expression profiling in deferasirox-treated K562 cells clarified up-regulation of several pathways which may reflect molecular mechanisms of iron chelator in human myeloid leukemia cells. The most prominent molecular feature is the up-regulation of *CDKN1A* encoding $p21^{CIP}$, which is consistent with the observation by Fu *et al.*[23] Deferroxamine paradoxically up-regulated $P21^{CIP1/WAF1}$ mRNA and down-regulates protein expression due to inhibition of the translocation of the $P21^{CIP1/WAF1}$ pathway and the induction of ubiquitin-independent proteasome degradation. We also noticed another pathway related to interferon. Several investigators have reported a possible association of iron chelation and inferferon.[24–26] Regis *et al.* reporter that iron regulates T-lymphocyte sensitivity to the IFN-gamma/Signal transducer

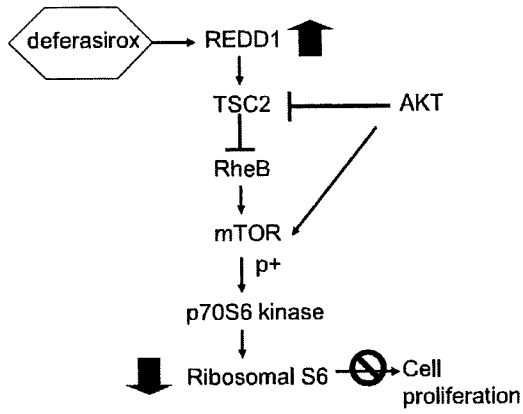


**Fig. 6.** Schematic model of REDD1/mTOR (mammalian target of rapamycin) pathways in deferasirox-treated K562 cells. The thicker arrow indicates the effect of deferasirox. When deferasirox is given, dephosphorylation of mTOR followed by up-regulation of the REDD1/tuberous sclerosis complex 2 (TSC2) pathway, induces down-regulation of ribosomal S6 protein, thereby, inhibiting cell proliferation.

and activator of transcription (STAT1) signaling pathway *in vitro* and *in vivo*.[24] More recently, Mori *et al.* found that expression of IFN-gammaR2 is restored by iron chelation, deferoxamine, and the increased expression of IFN-gammaR2 enhances the antiproliferative effect of IFN-gamma through induction of apoptosis in colon cancer cells.[26] Taking those findings together, the IFN pathway may partly be involved in the process of the anticancer effect during iron chelation.

In the current study, we found a novel pathway involving REDD1 which has recently been identified as a stress-response gene and is strongly induced by hypoxia,[27] (Fig. 6). REDD1 can activate the TSC2 protein:[28,29] TSC is composed of two proteins, TSC1 (also known as hamartin) and TSC2 (also known as tuberin), which function to integrate growth factors and cell stress responses. It has been shown that the major function of the TSC1/2 complex is to inhibit the checkpoint protein kinase mTOR,[28,30] a major regulator of cell death and proliferation. The mTOR enhances translational initiation in part by phosphorylating two major targets, the eIF4E binding protein (4E-BPs) and the ribosomal protein S6 (S6K1 and S6K2) that cooperate to regulate translational initiation rates.[30–33]

To the best of our knowledge, we have for the first time shown up-regulation of REDD1 expression in human leukemia cells treated with deferasirox. The REDD1 gene is strongly induced under hypoxic conditions in a hypoxia-inducible factor-1 (HIF-1)-dependent manner.[34] We demonstrated down-regulation of mTOR following up-regulation of REDD1, and marked down-regulation of the phosphorylated S6 protein in deferasirox-treated leukemia cells. Blockage of the REDD1 expression by siRNA resulted in restoration of mTOR and phosporylation of S6 protein in deferasirox-treated leukemia cells, indicating that the pathway involving mTOR might be important for cytotoxicity in the presence of iron chelating agents. These data provide valuable insights for novel therapeutic approaches aimed at the REDD1/mTOR pathway in human myeloid leukemia cells by means of iron chelation.

Although deferasirox may affect multiple pathways related to cell survival, more importantly, we demonstrated that deferasirox can induce apoptosis in xenotransplatable human leukemia cells in tumor-bearing mice. Our results may provide new insights into the complex molecular mechanism of iron chelation in human myeloid leukemia cells. Deferasirox might have benefit for not only iron chelation but also be an antiproliferative agent in some myeloid leukemia cells, especially in patients with myelodysplastic syndrome who need both iron chelation and reduction of leukemia cells.

## Acknowledgments

The authors are indebted to Professor J. Patrick Barron of the International Medical Communications Center of Tokyo Medical University for his review of this manuscript. The authors also wish to thank Mr Yoshinobu Kamimura for his technical assistance. This work was supported by the 'Strategic Research Based Support' Project for private universities: matching fund subsidy from the MEXT (Ministry of Education, Culture, Sports, Science and Technology, 2008–12), and by the 'University-Industry Joint Research Project' for private universities: matching fund subsidy from the MEXT, 2007–09 (to KO, JHO).

## References

1 Zhang AS, Enns CA. Iron homeostasis: recently identified proteins provide insight into novel control mechanisms. *J Biol Chem* 2008; August 29 [Epub ahead of print].
2 Andrews NC. Forging a field: the golden age of iron biology. *Blood* 2008; **112**: 219–30.
3 Domenico I, McVey Ward D *et al.* Regulation of iron acquisition and storage: consequences for iron-linked disorders. *Nat Rev Mol Cell Biol* 2008; **9**: 72–81.
4 Brard L, Granai CO, Swamy N. Iron chelators deferoxamine and diethylenetriamine pentaacetic acid induce apoptosis in ovarian carcinoma. *Gynecol Oncol* 2006; **100**: 116–27.
5 Yu Y, Wong J, Lovejoy DB *et al.* Chelators at the cancer coalface: desferrioxamine to Triapine and beyond. *Clin Cancer Res* 2006; **12**: 6876–83.
6 Kalinowski DS, Sharpe PC, Bernhardt PV *et al.* Design, synthesis, and characterization of novel iron chelators: structure-activity relationships of the 2-benzoypyridine thiosemicarbazone series and their 3-nitrobenzoyl analogues as potent antitumor agents. *J Med Chem* 2007; **50**: 3716–29.
7 Triantafyllou A, Liakos P, Tsakalof A *et al.* The flavonoid quercetin induces hypoxia-inducible factor-1alpha (HIF-1alpha) and inhibits cell proliferation by depleting intracellular iron. *Free Radic Res* 2007; **41**: 342–56.
8 Gharagozloo M, Khoshdel Z, Amirghofran Z. The effect of an iron (III) chelator, silybin, on the proliferation and cell cycle of Jurkat cells: a comparison with desferrioxamine. *Eur J Pharmacol* 2008; **589**: 1–7.
9 Cilloni D, Rosso V, Messa E *et al.* The oral ironchelator ICL670 is a otent inhibitor of NF-KB and this activity is independent from iron overload in MDS cells. *Haematologica* 2007; **s1**: 238.
10 Messa E, Defilippi I, Roetto A *et al.* Deferasirox is the only iron chelator acting as a potent NF-KB inhibitor in myelodysplastic syndromes. *Blood* (50th ASH Annual Meeting and and Exposition: 2008, Dec 6 to 9, San Francisco), abstract # 2671.
11 Choudhari SR, Khan MA, Harris G *et al.* Deactivation of Akt and STAT3 signaling promotes apoptosis, inhibits proliferation, and enhances the sensitivity of hepatocellular carcinoma cells to an anticancer agent, Atiprimod. *Mol Cancer Ther* 2007; **6**: 112–21.
12 Zhang Y, Ohyashiki JH, Takaku T *et al.* Transcriptional profiling of Epstein-Barr virus (EBV) genes and host cellular genes in nasal NK/T-cell lymphoma and chronic active EBV infection. *Br J Cancer* 2006; **94**: 599–608.
13 Ohyashiki JH, Hisatomi H, Nagao K *et al.* Quantitative relationship between functionally active telomerase and major telomerase components (hTERT and hTR) in acute leukaemia cells. *Br J Cancer* 2005; **92**: 1942–7.
14 Ohyashiki JH, Hamamura R, Kobayashi C, Zhang Y, Ohyashiki K. A network approach for anti-cancer effect of bortezmib identifies SPARC as a therapeutic target in adult T-cell leukemia cells. *Computational Biol Chem Adv Appl* 2008; **1**: 85–93.
15 Akahane D, Tauchi T, Okabe S *et al.* Activity of a novel Aurora kinase inhibitor against the T315I mutant form of BCR-ABL. in vitro and in vivo studies. *Cancer Sci* 2008; **99**: 1251–7.
16 Richardson DR, Tran EH, Ponka P. The potential of iron chelators of the pyridoxal isonicotinoyl hydrazone class as effective antiproliferative agents. *Blood* 1995; **86**: 4295–306.
17 Valle P, Timeus F, Piglione M *et al.* Effect of different exposures to desferrioxamine on neuroblastoma cell lines. *Pediatr Hematol Oncol* 1995; **12**: 439–46.
18 Darnell G, Richardson DR. The potential of iron chelators of the pyridoxal isonicotinoyl hydrazone class as effective antiproliferative agents III. the effect of the ligands on molecular targets involved in proliferation. *Blood* 1999; **94**: 781–92.
19 Chaston TB, Lovejoy DB, Watts RN *et al.* Examination of the



doi: 10.1111/j.1349-7006.2009.01131.x

antiproliferative activity of iron chelators: multiple cellular targets and the different mechanism of action of triapine compared with desferrioxamine and the potent pyridoxal isonicotinoyl hydrazone analogue 311. *Clin Cancer Res* 2003; **9**: 402–14.
20 Lescoat G, Chantrel-Groussard K, Pasdeloup N *et al.* Antiproliferative and apoptotic effects in rat and human hepatoma cell cultures of the orally active iron chelator ICL670 compared to CP20: a possible relationship with polyamine metabolism. *Cell Prolif* 2007; **40**: 755–67.
21 Chantrel-Groussard K, Gaboriau F *et al.* The new orally active iron chelator ICL670A exhibits a higher antiproliferative effect in human hepatocyte cultures than O-trensox. *Eur J Pharmacol* 2006; **541**: 129–37.
22 Miyazawa K, Ohyashiki K, Urabe A *et al.* A safety, pharmacokinetic and pharmacodynamic investigation of deferasirox (Exjade, ICL670) in patients with transfusion-dependent anemias and iron-overload: a Phase I study in Japan. *Int J Hematol* 2008; **88**: 73–81.
23 Fu D, Richardson DR. Iron chelation and regulation of the cell cycle: 2 mechanisms of posttranscriptional regulation of the universal cyclin-dependent kinase inhibitor $p21^{CIP1/WAF1}$ by iron depletion. *Blood* 2007; **110**: 752–61.
24 Regis G, Bosticardo M, Conti L *et al.* Iron regulates T-lymphocyte sensitivity to the IFN-gamma/STAT1 signaling pathway in vitro and in vivo. *Blood* 2005; **105**: 3214–21.
25 Okada T, Sawada T, Kubota K. Deferoxamine enhances anti-proliferative effect of interferon-gamma against hepatocellular carcinoma cells. *Cancer Lett* 2007; **248**: 24–31.
26 Mori S, Sawada T, Okada T, Kubota K. Anti-proliferative effect of interferon-gamma is enhanced by iron chelation in colon cancer cell lines in vitro. *Hepatogastroenterology* 2008; **55**: 1274–9.
27 Schwarzer R, Tondera D, Arnold W *et al.* REDD1 integrates hypoxia-mediated survival signaling downstream of phosphatidylinositol 3-kinase. *Oncogene* 2005; **24**: 1138–49.
28 Nobukini T, Thomas G. The mTOR/S6K signalling pathway. the role of the TSC1/2 tumour suppressor complex and the proto-oncogene Rheb. *Novartis Found Symp* 2004; **262**: 148–54; discussion 154–9, 265–8.
29 Wang H, Kubica N, Ellisen LW *et al.* Dexamethasone represses signaling through the mammalian target of rapamycin in muscle cells by enhancing expression of REDD1. *J Biol Chem* 2006; **281**: 39128–34.
30 Li Y, Corradetti MN, Inoki K *et al.* filling the GAP in the mTOR signaling pathway. *Trends Biochem Sci* 2004; **29**: 32–8.
31 Corradetti MN, Inoki K, Guan KL. The stress-inducted proteins RTP801 and RTP801L are negative regulators of the mammalian target of rapamycin pathway. *J Biol Chem* 2005; **280**: 9769–72.
32 Jin HO, An S, Lee HC *et al.* Hypoxic condition- and high cell density-induced expression of Redd1 is regulated by activation of hypoxia-inducible factor-1alpha and Sp1 through the phosphatidylinositol 3-kinase/Akt signaling pathway. *Cell Signal* 2007; **19**: 1393–403.
33 Wang H, Kubica N, Ellisen L *et al.* Dexamethasone represses signaling through the mammalian target of Rapamycin in muscle cells by enhancing expression of REDD1. *J Biol Chem* 2006; **51**: 39128–34.
34 Wouters BG, Koritzinsky M. Hypoxia signalling through mTOR and the unfolded protein response in cancer. *Nat Rev Cancer* 2008; **8**: 851–64.
35 Shoshani T, Faerman A, Mett I *et al.* Identification of a novel hypoxia-inducible factor 1-responsive gene, RTP801, involved in apoptosis. *Mol Cell Biol* 2002; **22**: 2283–93.

## Supporting Information

Additional Supporting Information may be found in the online version of this article:

**File S1.** Western blot analysis of U937 and HL60 with or without treatment by deferasirox: Expression of phosphorylated S6 ribosomal protein was decreased in the presence of deferasirox.

Please note: Wiley-Blackwell are not responsible for the content or functionality of any supporting materials supplied by the authors. Any queries (other than missing material) should be directed to the corresponding author for the article.

Leukemia Research 33 (2009) 756–758

Contents lists available at ScienceDirect

Leukemia Research

journal homepage: www.elsevier.com/locate/leukres

# Evaluation of cardiac iron overload in transfusion-dependent adult marrow failure patients by magnetic resonance imaging

Jinho Park[a], Kazuma Ohyashiki[b,*], Soichi Akata[a], Kenichi Takara[a], Ritsuko Uno[a], Dai Kakizaki[a], Keisuke Miyazawa[b], Yukihiko Kimura[b], Koichi Tokuuye[a]

[a] Department of Radiology, Tokyo Medical University, Tokyo 160-0023, Japan
[b] First Department of Internal Medicine (Division of Hematology), Tokyo Medical University, 6-7-1 Nishishinjuku, Shinjuku-ku, Tokyo 160-0023, Japan

ARTICLE INFO

*Article history:*
Received 2 September 2008
Received in revised form 14 October 2008
Accepted 20 October 2008
Available online 26 November 2008

*Keywords:*
Iron overload
Myocardial evaluation
MRI
Transfusion-dependent

ABSTRACT

We investigated magnetic resonance imaging T2-star (MRI-T2*) values and left ventricular ejection fraction (LVEF) in 7 adult patients with bone marrow failure with heavy transfusion to elucidate the correlation between cardiac iron overload and dysfunction. We demonstrated a positive correlation between the total volume of red blood cells (RBC) transfusion and ejection fraction. The normal T2* limit value, which represents cardiac siderosis, is probably 200 mL/kg RBC transfusion. Patients with serum ferritin levels of under 5000 ng/mL and who received 200–400 mL/kg RBC transfusion showed mild but progressive decrease of the T2* value without obvious reduction of the ejection fraction, indicating that the T2* value of MRI could be a predictor for cardiac iron deposition before the appearance of myocardial dysfunction. Transfused RBC amount of >400 mL/kg or rapid elevation of ferritin level of >5000 ng/mL might be warning sign for critical cardiac dysfunction. Since iron overload of the heart is a major factor affecting co-morbidity of bone marrow failure, MRI evaluation of cardiac iron overload and functional disturbance in adult non-thalassemic patients is essential.



## 1. Introduction

Iron overload is a major problem in managing patients with bone marrow failure syndromes, since it has been clarified that cardiac dysfunction is a major life-threatening co-morbidity [1]. Takatoku et al. demonstrated that most of the deaths of iron overload adult patients with marrow failure syndromes were due to infection and leukemia; while cardiac and liver failure were noted in 24.0% and 6.7%, respectively [1]. Therefore, early detection of cardiac iron overload before apparent cardiac dysfunction, and chelation therapy for patients receiving heavy transfusion with acquired anemia is recommended. In the past, a limited number of studies regarding myocardial iron overload in adult patients with transfusion-dependent acquired anemias have been published [2–7]. Some reports suggested that the cardiac magnetic resonance imaging T2-star (MRI-T2*) technique could be useful in determining cardiac iron overload [3,7], while the efficacy of MRI is still controversial [2]. We, therefore, planned to address this relevant clinical issue.

## 2. Materials and methods

### 2.1. Patients

We studied 7 adult patients with hematologic diseases, all of whom were transfusion-dependent. Total red cell transfusion value at the time of MRI evaluation ranged from 64 (12,800 mL) to 242 (48,400 mL) Japanese units (1 unit = 200 mL) of red blood cells (RBC). Serum ferritin levels ranged from 2868 ng/mL to 17,547 ng/mL at the time of the MRI study. Of the 7 patients, 2 each was given a diagnosis of diabetes mellitus or liver dysfunction (Table 1). None of the patients in this study received oral chelation therapy, but all of them received intermittent intravenous deferoxamine therapy.

### 2.2. MRI evaluation

We used a Magnetom Avanto 1.5 T scanner (Siemens AG, Erlangen, Germany) using a gradient echo T2* MRI technique. Gradient echo (GRE) T2*WI, and true-fast imaging with steady-state procession (true FISP) sequence was applied for a single mid-ventricular short-axis slice of the left cardiac ventricle at seven echo times (5 ms, 7 ms, 10 ms, 13 ms, 15 ms, 17 ms and 20 ms). The repeat time between each radiofrequency pulse was 170 ms. Phased array coils, electrocardiogram (ECG) gating, and breath holding methods were also utilized. We selected the short-axis of the left cardiac ventricle and applied true-FISP sequence to obtain cine MRI.

All MRI data were analyzed using Argus soft ware (Siemens AG) to calculate left ventricular ejection fraction (LVEF). Regions of interest (ROI) were set to the left ventricle wall. Measured signal intensity was fitted for an exponential curve and we obtained the T2* value of the myocardium. Axial T2*WI of upper abdomen was also obtained to determine the amounts of iron deposition in other organs, including the liver, pancreas, spleen, and vertebrae.

* Corresponding author. Tel.: +81 3 3342 1510; fax: +81 3 5381 6651.
*E-mail address:* ohyashik@rr.iij4u.or.jp (K. Ohyashiki).

0145-2126/$ – see front matter © 2008 Elsevier Ltd. All rights reserved.
doi:10.1016/j.leukres.2008.10.018

**Table 1**
Clinico-hematologic characteristics of patients with iron overload.

| UPN | Age (yo)/sex | Diagnosis | Hb (g/dL) | Platelets ($\times 10^6$/L) | Total RBC transfusion (Japanese unit) | Serum ferritin (ng/mL) | Fe (μg/dL) | T2* value (ms) | LVEF (%) |
|---|---|---|---|---|---|---|---|---|---|
| 1 | 56/male | MDS-RAEBt | 7.7 | 31 | 12,800 mL (64) | 3,056 | 171 | 94.34 | 61 |
| 2 | 71/female | MDS-RA | 5.1 | 158 | 32,000 mL (160) | 16,987 | 334 | ND | 52.8 |
| 3 | 66/male | MDS-RA | 7.9 | 15 | 23,200 mL (116) | 3,856 | ND | 35.71 | 63 |
| 4 | 37/female | AA | 7.9 | 3 | 48,400 mL (242) | 17,547 | 379 | 11.55 | 26.5 |
| 5 | 52/female | AA | 8.2 | 11 | >12,800 mL (>64) | 3,441 | 233 | 50 | 54.8 |
| 6 | 77/male | PMF | 7.2 | 34 | 11,600 mL (58) | 2,868 | 152 | 51.02 | 59.5 |
| 7 | 71/male | PMF | 4.6 | 212 | 24,000 mL (120) | 3,176 | 300 | 35.59 | 61.3 |

Disease: MDS-RA, myelodysplastic syndrome-refractory anemia; MDS-RAEBt, myelodysplastic syndrome-refractory anemia with excess blasts in transformation; AA, aplastic anemia; PMF, primary myelofibrosis. Patient 5 had a diagnosis at childhood, thus exact transfused amount is unclear.

## 3. Results

Left ventricular ejection fraction in the 7 patients ranged from 26.5% to 63% (normal range: 56–78% by MRI), with 3 (patient nos. 2, 4, and 5) of them being below the normal range. Two (patient nos. 2 and 4) of the 3 patients with reduced LVEF levels had heavy RBC transfusion of >160 Japanese units and the serum ferritin levels were >15,000 ng/mL. Although the remaining 4 transfusion-dependent patients showed ferritin levels of around 3000 ng/mL, none of them showed marked reduction of LVEF, except patient 5 who was given a diagnosis of aplastic anemia in childhood and in whom the exact transfused RBC amount could not be calculated.

Because of blurring artifacts, we measured cardiac T2* value in 6 patients. Breath holding was difficult for patient no. 2 and we therefore failed to establish the ROI in the myocardium of this patient. Although the number of patients in this study is too small to provide a definite conclusion, we were able to note some tendencies regarding iron overload in the heart. Two patients (nos. 1 and 6) who received relatively small amounts of RBC transfusions (approximately 60 Japanese units: 12,000 mL) had normal T2* value, suggesting that at 60 units RBC (200 mL/kg) transfusion myocardial iron overload may not occur. Most patients with RBC transfusion of 60–120 units (200–400 mL/kg) maintained normal LVEF, while some of them demonstrated mild reduction in T2* value (35.71 ms and 35.59 ms); but the above 2 patients (nos. 3 and 7) with 60 units of transfusion showed the limit of the normal range T2* value reported by Anderson et al., i.e., 52 ± 16 ms [7]. These data indicate that some patients with heavy transfusion of 60–120 RBC Japanese units (12,000–24,000 mL RBC) may not be detectable myocardial damage by LVEF alone, and the T2* value of MRI could show cardiac iron deposition before the appearance of myocardial dysfunction.

We utilized GraphPad Prism 5.0 software (GraphPad Software Inc., San Diego, CA, USA) to obtain non-lineal fitting capabilities between total transfused RBC volume and serum ferritin, T2* value, or ejection fraction by MRI (Fig. 1).

(1) *No obvious cardiac siderosis*: patients with RBC transfusion of <200 mL/kg (<12,000 mL RBC) exhibiting elevated serum ferritin up to 4000 ng/mL, normal T2* value (36–68 ms), and normal LVEF (56–78% by MRI).
(2) *Cardiac siderosis*: patients with RBC transfusion of 200–400 mL/kg (12,000–24,000 mL RBC) exhibiting elevated serum ferritin up to 4000 ng/mL, progressive reduction of the T2* value, and normal LVEF (56–78% by MRI).
(3) *Cardiac dysfunction due to siderosis*: patients with RBC transfusion of >400 mL/kg (>24,000 mL) exhibiting elevated serum ferritin levels of more than 15,000 ng/mL, reduced T2* value (<20 ms), and abnormal LVEF (<56% by MRI).

## 4. Discussion

In the current study, we failed to demonstrate a linear correlation between the T2* value and left ventricular ejection fraction, especially in patients with transfusion of less than 120 Japanese units of RBC (<400 mL/kg). Approximately 50% of them showed some reduction of T2* value, while most of them exhibited a normal LVEF, indicating that these high transfusion level patients are at high risk for developing cardiac dysfunction, and detection of insidiously progressive dysfunction detected by MRI might be important for those patients. The situation is similar in those with serum ferritin levels between 2000 ng/mL and 4000 ng/mL: evaluation of LVEF alone by echocardiogram may fail to find out the pre-existing myocardial damage due to iron overload.

The T2* value is related to not only iron deposition but also fibrosis, and MRI reflects total images of these pathologic changes. Currently iron chelation therapy for hematologic disease patients, especially those with myelodysplastic syndromes (MDS), with transfusion-dependency is recommended [3], and definitions of iron overload for MDS patients have been proposed [8,9]. Although the starting point for iron chelation therapy is proposed, the exact evaluation of iron overload and functional estimation in each organ is probably important. Reduction of iron deposition in mouse organs by chelation therapy was demonstrated [10]. Thus, improvement of cardiac siderosis and myocardial dysfunction by chelation therapy should be determined.

Anderson et al. reported cardiac iron deposition in 109 thalassemia patients with iron chelation therapy and found significant ventricular dysfunction in patients with myocardial T2* values of less than 20 ms, and progressive decline in ejection fraction [7].

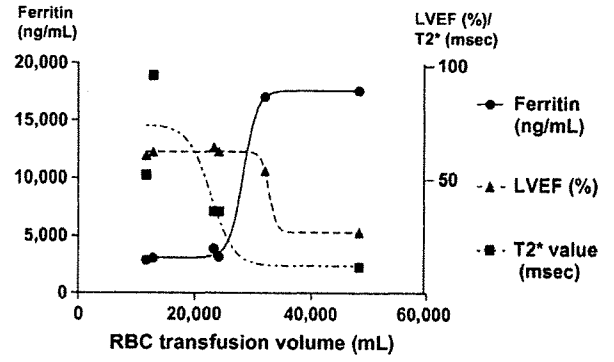


**Fig. 1.** Correlation between total units of red blood cell transfusion (horizontal axis) and left ventricular ejection fraction (LVEF), serum ferritin, and cardiac T2* value using GraphPad Prism 5.0 software. Rapid decline of T2* value, but stable LVEF within the normal range until 400 mL/kg of red blood cell transfusion and serum ferritin level of <5000 ng/mL are notable. The rapid decline of LVEF following rapid elevation of serum ferritin is evident.

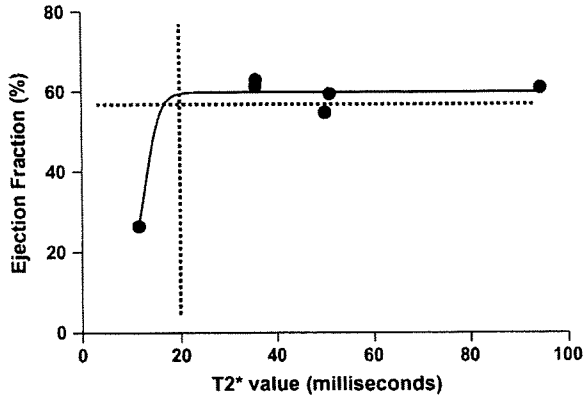


**Fig. 2.** Correlation between cardiac T2* value and left ventricular ejection fraction. The vertical dotted line indicates the cut-off value of T2* (20 ms) and the horizontal dotted line shows the cut-off value of LVEF (56%) for cardiac dysfunction.

In contrast, Jensen et al. failed to demonstrate significant correlation between cardiac T2* value and serum ferritin levels [5]. More recently, Di Tucci et al. reported myocardial iron overload detected by MRI in adult transfusion-dependent acquired anemias and found cardiac T2* value correlated with transfusion burden, and suggested that 290 mL/kg RBC might be a cut-off for myocardial damage [6]. Our results show that patients who received transfusions of up to 24,000 mL RBC (approximately 400 mL/kg) had a progressive decrease of the T2* value, but most of them had a normal left ventricular ejection fraction. These data clearly indicate that patients receiving 200–400 mL/kg RBC transfusion with moderate reduction of T2* value, but not less than 20 ms, in acquired anemia patients with heavy transfusion may be at high risk for progressive cardiac dysfunction (Fig. 2).

In conclusion, RBC transfusion of 200 mL/kg RBC might be the limit for monitoring normal T2* values. Patients who received 200–400 mL/kg RBC transfusion showed progressive decrease of T2* value without obvious reduction of ejection fraction, indicating that the T2* value of MRI could indicate cardiac iron deposition before apparent myocardial dysfunction. Patients who had received ≥400 mL/kg RBC transfusion eventually showed progressive cardiac failure.

## Conflicts of interest

The authors declare no conflicts of interests.

## Acknowledgements

Thanks are due to Prof. J. Patrick Barron, salaried employer of Tokyo Medical University, for his review of this manuscript. We also thank to Mr. H. Katsuyama and Y. Araki, Department of Radiology, Tokyo Medical University, Y. Komori, Siemens-Asahi Medical Technologies Ltd., Japan, for their technical help and Dr. J. H. Ohyashiki, Intractable Diseases Research Center, for statistical analysis. This work was supported in part by a Grant-in-Aid from Japanese Ministry of Health, Labor and Welfare.

## References

[1] Takatoku M, Uchiyama T, Okamoto S, et al. Japanese National Research Group on Idiopathic Bone Marrow Failure Syndromes. Retrospective nationwide survey of Japanese patients with transfusion-dependent MDS and aplastic anemia highlights the negative impact of iron overload on morbidity/mortality. Eur J Haematol 2007;78:487–94.
[2] Konen E, Ghoti H, Goitein O, et al. No evidence for myocardial iron overload in multitransfused patients with myelodysplastic syndrome using cardiac magnetic resonance T2 technique. Am J Hematol 2007;82:1013–6.
[3] Greenberg PL. Myelodysplastic syndromes: iron overload consequences and current chelating therapies. J Natl Compr Cancer Netw 2006;4:91–6.
[4] Chacko J, Pennell DJ, Tanner MA, et al. Myocardial iron loading by magnetic resonance imaging T2* in good prognostic myelodysplastic syndrome patients on long-term blood transfusions. Br J Haematol 2007;138:587–93.
[5] Jensen PD, Jensen FT, Christensen T, et al. Evaluation of myocardial iron by magnetic resonance imaging during iron chelation therapy with deferrioxamine: indication of close relation between myocardial iron content and chelatable iron pool. Blood 2003;101:4632–9.
[6] Di Tucci AA, Matta G, Deplano S, et al. Myocardial iron overload assessment by T2* magnetic resonance imaging in adult transfusion dependent patients with acquired anemias. Haematologica 2008;93:1358–8.
[7] Anderson LJ, Holden S, Davis B, et al. Cardiovascular T2-star (T2*) magnetic resonance for the early diagnosis of myocardial iron overload. Eur Heart J 2001;22:2171–9.
[8] Gatterman N. Guidelines on iron chelation therapy in patients with myelodysplastic syndromes and transfusional iron overload. Leuk Res 2007;(Suppl. 3):S10–5.
[9] Suzuki T, Tomonaga M, Miyazaki Y, et al. Japanese epidemiological survey with consensus statement on Japanese guidelines for treatment of iron overload in bone marrow failure syndromes. Int J Hematol 2008;88:30–5.
[10] Wood JC, Otto-Duessel M, Gonzalez I, et al. Deferasirox and deferiprone remove cardiac iron in the iron-overload gerbil. Transl Res 2006;148:272–80.

Biochemical and Biophysical Research Communications 383 (2009) 245–251

Contents lists available at ScienceDirect

Biochemical and Biophysical Research Communications

journal homepage: www.elsevier.com/locate/ybbrc

# Identification of a common microdeletion cluster in 7q21.3 subband among patients with myeloid leukemia and myelodysplastic syndrome

Hiroya Asou, Hirotaka Matsui, Yuko Ozaki, Akiko Nagamachi, Megumi Nakamura, Daisuke Aki, Toshiya Inaba *

*Department of Molecular Oncology and Leukemia Program Project, Research Institute for Radiation Biology & Medicine, Hiroshima University, 1-2-3 Kasumi, Minami-ku, Hiroshima 734-8553, Japan*

ARTICLE INFO

*Article history:*
Received 31 March 2009
Available online 7 April 2009

*Keywords:*
Monosomy 7
Myeloid malignancy
Tumor suppressor
Mitosis

ABSTRACT

Monosomy 7 and interstitial deletions in the long arm of chromosome 7 (−7/7q−) is a common nonrandom chromosomal abnormality found frequently in myeloid disorders including acute myeloid leukemia (AML), myelodysplastic syndrome (MDS), and juvenile myelomonocytic leukemia (JMML). Using a short probe-based microarray comparative genomic hybridization (mCGH) technology, we identified a common microdeletion cluster in 7q21.3 subband, which is adjacent to 'hot deletion region' thus far identified by conventional methods. This common microdeletion cluster contains three poorly characterized genes; *Samd9*, *Samd9L*, and a putative gene *LOC253012*, which we named *Miki*. Gene copy number assessment of three genes by real-time PCR revealed heterozygous deletion of these three genes in adult patients with AML and MDS at high frequency, in addition to JMML patients. Miki locates to mitotic spindles and centrosomes and downregulation of Miki by RNA interference induced abnormalities in mitosis and nuclear morphology, similar to myelodysplasia. In addition, a recent report indicated Samd9 as a tumor suppressor. These findings indicate the usefulness of the short probe-based CGH to detect microdeletions. The three genes located to 7q21.3 would be candidates for myeloid tumor-suppressor genes on 7q.



## Introduction

Monosomy 7 and interstitial deletions in 7q (−7/7q−) are a common nonrandom chromosomal abnormality found frequently in myeloid disorders. In 1964, prior to chromosome band identification, monosomy 7 was first reported in three patients with refractory anemia as monosomy of a C-group chromosome [1]. Since that time, −7/7q− have been identified in 10–20% of a wide range of myeloid malignancies including MDS, AML, and JMML [2].

Enormous efforts have been made to identify genes responsible for −7/7q−. In the absence of definitive familial cases, the basic strategy for gene hunting began with identifying patients that carried 7q−. Detailed maps of regions deleted from individual patients were then generated from the results of loss of heterogeneity assays or fluorescence *in situ* hybridization. Unfortunately, the cumulative results from thousands of patients were confounded by the fact that the boundaries of commonly deleted regions derived by separate research groups showed a poor degree of overlap [3]. Currently, it is generally accepted that two or more genes near bands 7q22 and/or 7q34 are involved in myeloid tumors.

Microarray-based comparative genomic hybridization (mCGH) technology allows efficient detection of microdeletions (<100 kb) that affect one or a few genes, enabling to search for small 7q deletions that are not visible cytogenetically in marrow cells of MDS/AML patients. Initially, bacterial artificial chromosome (BAC)-based mCGH systems were developed, but this system had limited potential to detect microdeletions because of the long probe size (>100 kb). Thereafter, SNP-array hybridization turned out to be a powerful method for detecting not only single nucleotide polymorphism, but also microdeletions [4]. However, because SNPs tend to cluster within introns and intergenic spaces, SNP-array may bias against the detection of microdeletions in critical genes.

Here, we describe the application of a modified BAC-based mCGH system that uses short (<10 kb) genomic DNA fragments without any repetitive sequences as probes to improve the detection of small deletions and reduce background hybridization. Because repeat-free fragments generally overlap exon-containing regions, this type of probe not only yields a high signal/noise ratio, but also can be useful in determining the copy number of a corresponding gene. Using this system for identification of responsible gene(s) for −7/7q−, we report the isolation of a common microde-

* Corresponding author. Fax: +81 82 256 7103.
*E-mail address:* tinaba@hiroshima-u.ac.jp (T. Inaba).

0006-291X/$ - see front matter © 2009 Elsevier Inc. All rights reserved.
doi:10.1016/j.bbrc.2009.04.004

letion among JMML patients that contains three poorly characterized genes.

## Materials and methods

*Short probe-based mCGH.* This system was similar to that described by others [5]. Briefly, total 292 repeat-free segments (2.7–9.5 kb) were identified using BlastN at the NCBI server (235 probes in 7q21.2–7q31.1, 15 in 4q12, 27 in 20q, and 15 in 21q). Each of these fragments was PCR amplified from human placenta DNA (Clontech, Mountain View, CA) and cloned into the pCR-XL-TOPO vector (Invitrogen, Carlsbad, CA). The primer sets used to amplify probes #14–#16 are listed in Table 1. Sequences of other primer sets are available upon request. Five micrograms of each target DNA, PCR-amplified fragments using universal primers in the vector, was printed on poly-L-lysine coated glass slides (Matsunami Glass, Osaka, Japan) using a spotter (SPBIO, Hitachi Software, Tokyo, Japan). Bone marrow samples were obtained after informed consent and approval from the Institutional Review Board at Hiroshima University. Test samples and reference placenta DNA (2.5 μg) were random-prime labeled with CY3- and CY5-dCTP (GE healthcare), respectively, and then hybridized to the slide. Scanning of microarrays was performed using G2505A scanner (Agilent Technologies, Santa Clara, CA) and signals were analyzed with ArrayVision (GE healthcare).

*Cell culture and gene transfer.* EOL-1 and MUTZ-3 cells ([6] and references in it) were cultured in RPMI1640 medium with 10% (FBS). 293 and HeLa(tc) [7] cells were cultured in Dulbecco's modified Eagle's medium supplemented with 10% fetal bovine serum (FBS). siRNA oligonucleotides (100 nM, otherwise indicated, Table 2) were transfected using Oligofectamine (Invitrogen). C-terminal FLAG-tagged Mikiα or β protein, or MikiΔN-FLAG(C) protein (lacking N-terminal hydrophobic 30 aa of Mikiβ) was expressed using the pcDNA3 expression vector (Invitrogen).

*Other experimental procedures and reagents.* Copy number assessment by qPCR was performed according to the procedure described [8]. qRT-PCR was performed as previously described [9] using primer sets (Table 1). Immunoprecipitation and immunoblot analyses were performed according to the standard procedures [10] using 2% gelatin as a blocking agent. Immunostaining and image analyses were performed as described [7,11]. Rabbit anti-Miki antibodies was raised against GST-Mikiα (377–462 aa) and affinity purified according to the standard procedures [10].

**Table 2**
Target sequences for RNAi.

| Name | Sequence |
|---|---|
| siRNA#79 | CGGUUGAUGAUCCUGUCAC |
| siRNA#80 | GGAAGACAUUGGGAAUUAC |
| siRNA#81 | AGGCAUUUAUGCAAAUUGAA |
| shMiki#1 | AUGCAUCUCUGCUUAUCAACC |
| shMiki#2 | GAAGGCAAUUACAUCGUGAAG |
| shMiki#3 | UCAGGGAAAUGGAACUCUAUC |
| shMiki#4 | AGAAGACAAUGGACUAUGUGU |
| shMiki#5 | GAAACUCAUUUCACAGUUAUC |
| shMiki#6 | UGACUUCGGAAUAUAUGAAUU |

## Results

*Identification of three candidate myeloid tumor-suppressor genes in a common microdeletion cluster among JMML patients*

Two hundred thirty-five probes in a region spanning 21.7 Mb within 7q21.2–7q31.1 and additional 57 control probes in 4q, 20q, and 21q were applied to a search for microdeletions using a short probe-based mCGH system (see Materials and methods). Test (leukemia) and reference DNA samples were labeled with CY3- and CY5-dCTP, respectively, and then hybridized to slides on which probes were printed.

We initially tested whether this system can detect copy number changes in a small region. Genomic DNA extracted from EOL-1 cells, which is known to harbor a deletion spanning 800 Kb between the *Rhe* (*FIP1L1*) gene and the *PDGFα* gene in 4q [12]. All eight probes (#239–#246) that locate within the deletion showed low fluorescence ratios (Fig. 1A, bracket), demonstrating the potential of this system to detect microdeletions. For detection of microdeletion in myeloid leukemia cells, we selected fresh bone marrow samples from adult AML/MDS patients or DNA from myeloid leukemia cell lines that did not show apparent 7q abnormalities. However, as shown, for an example, in Fig. 1B, gross regional copy number changes were still detected, and 'single copy events', which could include both real copy number changes in a small region and noise of the system, were frequently observed, recognized as general problems in detection of microdeletions in leukemia cells [13]. We then applied the microarray CGH system to samples from JMML patients, which is a subtype of MDS and is occasionally associated with monosomy 7 [2]. In contrast to adult MDS/AML pa-

**Table 1**
Primer sets.

| | Forward | Reverse |
|---|---|---|
| Probe#14 | 5′-AACTTCTCCTGACTCCAGTCATAGCTCCTT-3′ | 5′-ATCCATAGACCTGACATGTGTATCATATCC-3′ |
| Probe#15 | 5′-GTGGGAATCGTCTACTTCCTGCACTCAAGA-3′ | 5′-TGATTAAAGACTGGACCAAAGAGCATGTGA-3′ |
| Probe#16 | 5′-TGCTCACTCAACCGAAATCAATATTGAGAT-3′ | 5′-ATGCTTTAGGCTCCTAAGCCTTCTTTCCTT-3′ |
| Top2b | 5′-CAACTTTTTGCTGGCATCTG-3′ | 5′-GCTGGAATGTCTGGAAAAGC-3′ |
| Tel | 5′-ACAAATCACCGGCCTTCTCCTGACCC-3′ | 5′-GGCTGGATGGCTTCGGGTGGGACTC-3′ |
| Albumin | 5′-AGCTATCCGTGGTCCTGAAC-3′ | 5′-TTCTCAGAAAGTGTGCATATATCTG-3′ |
| c7orf16 | 5′-CAGGCCCAGCCTCGGTGAGC-3′ | 5′-GCACAACCCCGTGCCACCAG-3′ |
| DDC | 5′-CTCATGGCTCACGCGTCCAG-3′ | 5′-CAAGCCGACCTAGGTTGGTG-3′ |
| Cdk6 | 5′-ACACTGCCTTGTTGGCAAAG-3′ | 5′-AGGTTTGCAGAATCGAGGCC-3′ |
| Samd9–5′ | 5′-AACCCAGATATGGCTAATCC-3′ | 5′-CAGGTCTATGGATGGTTGCC-3′ |
| Samd9–3′ | 5′-CGTTTACAAGGTCGAGCTGA-3′ | 5′-CCCAGGTAAAAAGACACCTT-3′ |
| Samd9L | 5′-CATTCCTGTGCTTCTCCTTG-3′ | 5′-GGATTCCGGGATCTCATGCA-3′ |
| Miki-5′ | 5′-CCTGGTGAGGAACCCTGTCA-3′ | 5′-TCTCTGTGACTATCCTGGGA-3′ |
| Miki-3′ | 5′-CAAGGCATTCGGTTTGTAAG-3′ | 5′-CTCTGGTGAAGCAGAATTCT-3′ |
| CCDC132 | 5′-AGGATACCCTGGGTCGGCTC-3′ | 5′-TTCAGCCGCCGCGACTTACC-3′ |
| Col1A2 | 5′-GCAGTAACCTTATGCCTAGC-3′ | 5′-GAGAGTCTGCCCTCCAAGTG-3′ |
| Rint-1 | 5′-GCTGAGTATGTCTGTTGAAG-3′ | 5′-CCAAACTAGATACAGGTGCC-3′ |
| Lep | 5′-GTATCTCCAGGATTGAAGAG-3′ | 5′-CCCACTCTTTGCTGGGTGGA-3′ |
| Miki(RT) | 5′-AACTCTATCTGCCAGTCAGAAG-3′ | 5′-TTTAGCCATTGGTAAGCTAGCC-3′ |
| HPRT(RT) | 5′-CCTCATGGACTAATTATGGACAG-3′ | 5′-GCAGGTCAGCAAAGAATTTATAG-3′ |

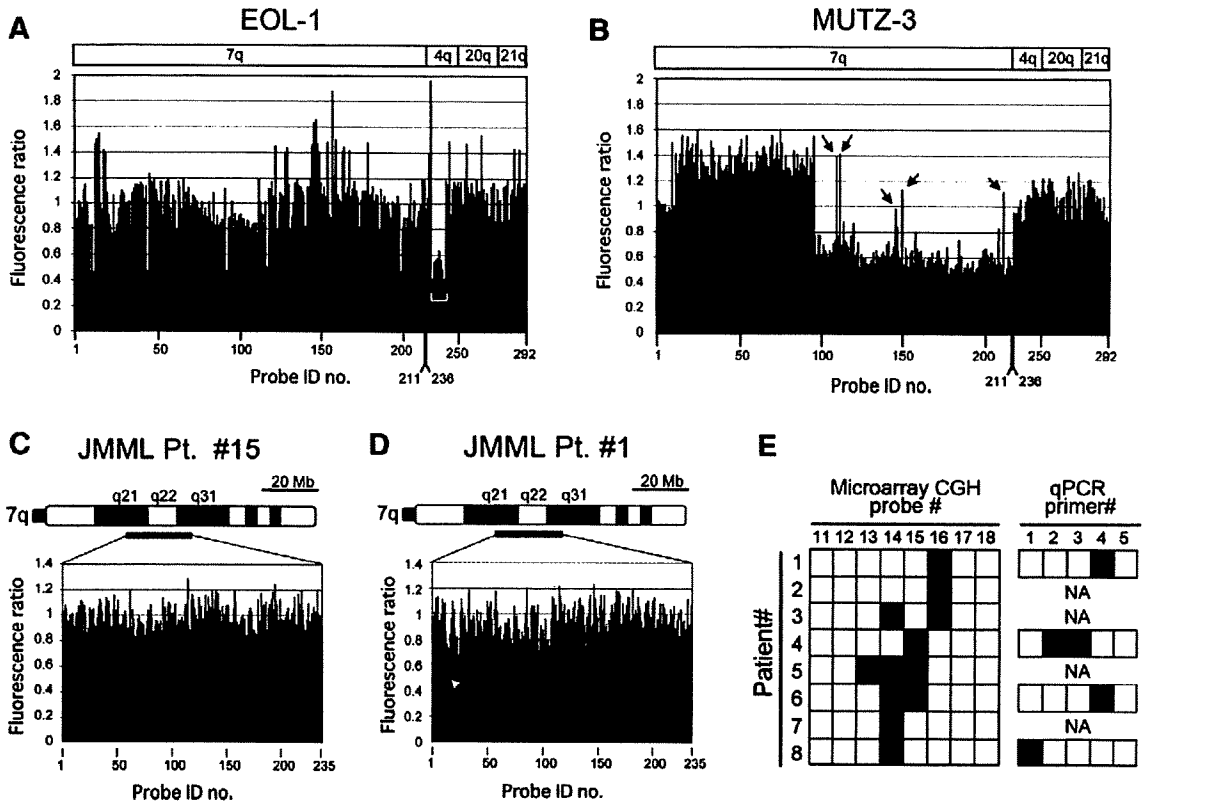


Fig. 1. Detection of microdeletions. (A–D) Profiles of short probe-based mCGHs. Normalized average fluorescence ratios by control placenta DNA (*Y*-axis) were derived from three replicates for each probe (*X*-axis). EOL-1 cells (A) which show reduced signals from eight probes located in a 4q12 microdeletion (bracket). A monocytic leukemia cell line MUTZ-3 (B); arrows indicate isolated copy number changes. JMML patients #15 (C) and #1 (D); an arrow shows reduced signals with probe #16. (E) Deletion profile summary for eight JMML patients using microarray CGH probes (#11–#18, left) and qPCR primer sets (#1–#5, right). Black boxes indicate a deletion in one allele. NA, samples not available.

tients and cell lines, JMML patients mostly carried no gross regional copy number changes nor single copy events (Fig. 1C). However, three contiguous probes (#14–#16) in the 7q21.2–21.3 subband were repeatedly found to show a low fluorescence ratio (Fig. 1D). In eight of the 21 JMML patients with normal karyotype, at least one of these three probes detected a microdeletion in one allele (Fig. 1E, left), suggesting that a region containing these probes is deleted frequently in JMML.

Three contiguous genes (*Samd9*, *Samd9L*, and *LOC253012*) identified by the human genome sequencing consortium (http://www.ncbi.nlm.nih.gov/) were found to overlap probes #14–#16, respectively (Fig. 2A). This region does not contain any known copy number polymorphisms (CNPs) [14], nor does it represent any microRNA sequence in miRBase [15] (http://microrna.sanger.ac.uk/).

To confirm the presence of a microdeletion cluster in chromosome 7 of JMML patients, we prepared five primer sets for real-time quantitative PCR analyses (qPCR) that efficiently amplify DNA fragment to allow estimating the copy number of each of these three genes (Fig. 2A) [8]. One allele loss of either one of the three genes was detected in all four patients whose DNA samples were available (Fig. 1E, right). We then extended the qPCR copy number assessment to 65 adult AML or MDS patients with diploid or near-diploid karyotype using the five primer sets for the three genes and additional sets for control genes on chromosome 7 and other chromosomes (Fig. 2B). Nearly 25% (15/61) of patients showed loss of one allele in at least one of the three genes (Fig. 2C), indicating that these three genes are heterozygously deleted at high frequency in both adult and childhood myeloid leukemia. In contrast to the chromosome 7 microdeletions among JMML patients (Fig. 1D), these three genes are more commonly lost with larger deletions in adult MDS/AML patients (Fig. 2D).

### *Miki-downregulation induced mitotic arrest and abnormal nuclear morphology*

Among the three genes, we named a putative gene *LOC253012 Miki* (mitotic kinetics regulator), because of the function of the gene product described below. Candidate *Miki* orthologues were identified in other vertebrates by search of Ensemble Genome Browser (http://www.ensembl.org/index.html), but not in invertebrates, plants, yeast, or prokaryotes. Miki transcript was detected on a Northern blot as a single 2.6 kb band in kidney and small intestine RNA with very weak signals, suggesting relatively low expression (data not shown). However, two alternatively splicing Miki messages, Mikiα (LOC253012 transcript variant-1, Genbank Accession No. NM_001039372) and Mikiβ (variant-2, NM_198151), which are derived from separate first coding exons (1a and 1b, Fig. 2A), were readily amplified by RT-PCR analyses of all examined organs (data not shown). Mikiα and Mikiβ transcripts encode distinctive 26- and 14-amino acid (aa) N-termini, respectively, which precede the same 436-aa C-terminal sequence (Fig. 3A).

Both Miki polypeptides encode three domains suggestive of cell surface proteins: an N-terminal hydrophobic region, a central region homologous to the immunoglobulin superfamily cell adhesion molecule, and a transmembrane domain-like region. Unexpectedly, immunostaining of HeLa cells using antibodies against the C-terminus of Miki showed an intense signal in the perinuclear re-

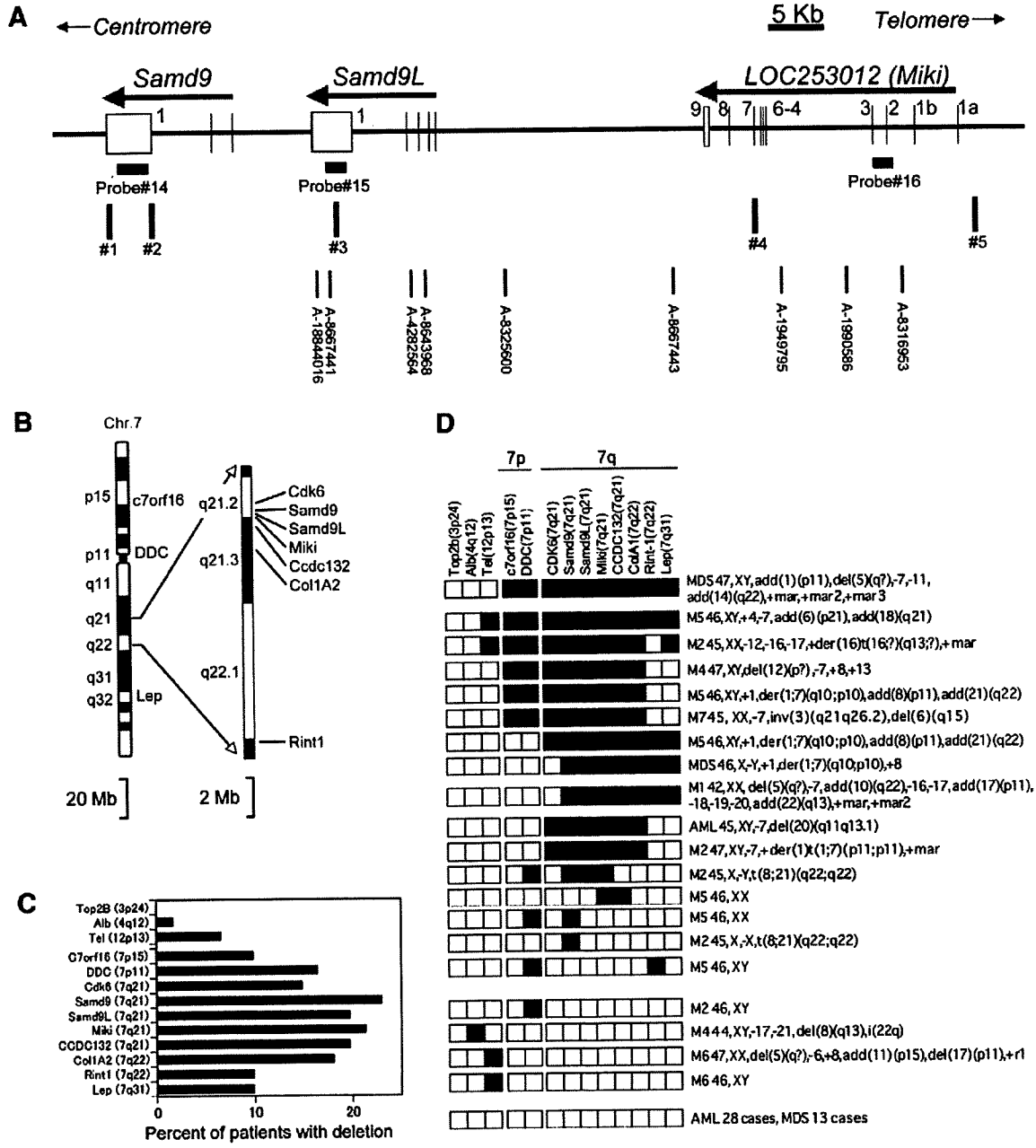


Fig. 2. Isolation of *Samd9*, *Samd9L*, and *Miki*. (A) A map of 7q21.3. The relative locations of exons for the three genes are depicted as boxes with coding exon numbers above. The positions of probes used in mCGH (#14–#16) and primer sets used for qPCR (#1–#5) are shown below. The positions of SNP probes in a SNP-array system (Genome-Wide SNP6.0) are also shown (bottom). (B–C) Percent of patients with adult MDS/AML (C) who lack one allele of each of the genes indicated in the diagram (C). Results of qPCR study (C). (D) Deletion profile summary of qPCR data from adult MDS/AML patients. Each column of boxes corresponds to results from a patient whose diagnosis and karyotype are indicated in the right. Black boxes indicate a deletion in one allele.

gion (Fig. 3B, left), which co-localized with Golgi-markers such as Golgin-97 in the interphase (middle). In mitosis, Miki immunostaining localized to centrosomes/spindles (right).

Miki seems to be modified post-translationally in a complex way. Four major bands were detected in immunoblots of 293-cell extracts with anti-Miki antibody (Fig. 3C, lane 1). The migration of the fastest band agreed with the predicted molecular mass (50 kDa). In contrast, transient expression of plasmid pcDNA3-Mikiβ-FLAG(C) generated C-terminal FLAG-tagged Mikiβ proteins that migrated as a broad band between 75 and 95 kDa (lane 2). Because peptide *N*-glycosidase F (PNGaseF) treatment of immunoprecipitated products from the transfected cells altered the migration of these bands to 50 kDa (lanes 3–5). Treatment of transfected cells with tunicamycin, a glycosylation inhibitor, also shifted the broad band to 50 kDa (lanes 6–7), suggesting that this broad band represents glycosylated forms of Miki. In transfected cells, exogenously expressed Mikiα protein also migrated as a broad band (lane 8); however, expression of MikiΔN-FLAG(C) (which lacks the N-terminal hydrophobic region) produced only one band that migrated slightly faster than p50 (lane 9), suggesting that Miki's N-terminal region functions as a signal peptide. The same blot analyzed with anti-FLAG antibody confirmed the identities of the broad band of

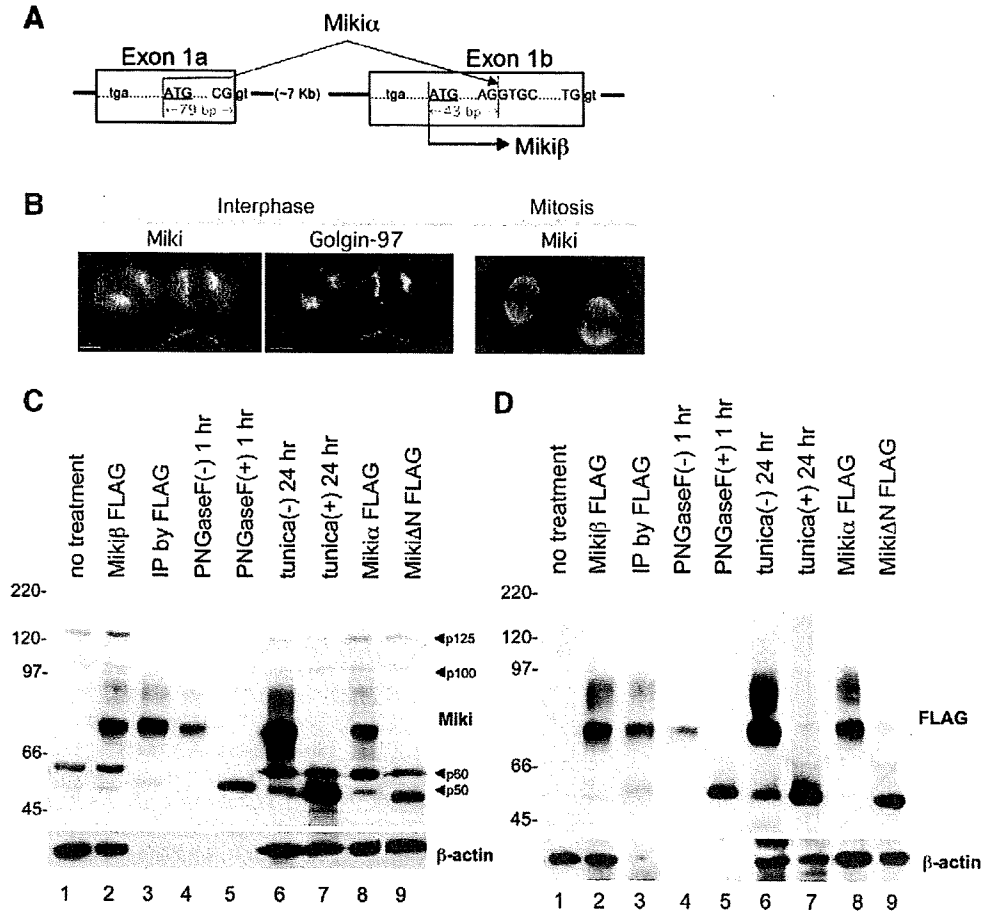


**Fig. 3.** Expression and localization of Miki. (A) Diagram of *Miki* gene structure. The initiation codon for Mikiα or Mikiβ is located in exon 1a or 1b, respectively. The Mikiα transcript is spliced using a cryptic splice acceptor in exon 1b. Exons 1a and 1b both encode *in frame* stop codons (tga) upstream of the initiation codons. The 5′ ends of exons 1a and 1b have not yet been determined. (B) Immunostaining of HeLa cells with Miki (FITC) and Golgin-97 (PE). Interphasic (left and middle), and mitotic cells (right). (C,D) Immunoblot analysis using Miki (C, top), FLAG (D, top) or β-actin (bottom) antibodies. Lane 1, untreated 293 cells; lane 2, cells transfected with pcDNA3-Mikiβ-FLAG(C); lane 3, anti-FLAG immunoprecipitates of cells transfected with pcDNA3-Mikiβ-FLAG(C); lanes 4–5, anti-FLAG immunoprecipitates incubated for 1 h in the absence or presence of PNGaseF; lanes 6–7, cells transfected with pcDNA3-Mikiβ-FLAG(C) cultured in the absence or presence of tunicamycin (1 μg/ml); lanes 8–9, cells transfected with pcDNA3-Mikiα-FLAG(C) or pcDNA3-MikiΔN-FLAG(C).

exogenous Miki protein (Fig. 3D, lanes 2–3, 6, 8), as well as deglycosylated Miki (lanes 5, 7) or MikiΔN protein (lane 9).

Because transient expression of Miki from a variety of virus-derived or eukaryotic promoters resulted uniformly in glycosylated protein, we predict that exogenously expressed Miki is altered by cryptic glycosylation events. In view of these results with Miki overexpression, we applied RNA interference to downregulate endogenous Miki. Six candidate Miki-specific short hairpin RNA (shRNA) sequences were selected and corresponding shRNA-expressing vectors [piGENE-mU6(neo)-hMiki#1–#6] were prepared. Immunoblot analysis of 293 cells co-transfected with pcDNA3-Mikiβ-FLAG(C) and each one of the six shRNA-expressing vectors demonstrate that three shRNAs (#1, #3, and #6) downregulated levels of glycosylated Miki efficiently (Fig. 4A). When cells were transfected with the shRNA-expressing vectors alone, shRNAs expressed from piGENE-mU6(neo)-hMiki#1, #3, or #6 also downregulated steady-state levels of endogenous Miki p125 and p50 (and p100 and p60 less effectively) (Fig. 4B).

In an alternate experiment, three Miki-based short interference RNAs (siRNAs) reduced steady-state levels of Miki mRNA to varying degrees when transfected directly into 293 cells (Fig. 4C). Immunoblots prepared from these cells showed that the intensities of Miki p125 and p50 signals (and p100 and p60 less effectively) were attenuated within 48 h of transfection with siRNA#79 or siRNA#80 (Fig. 4D), but not by siRNA#81 and control siRNA. These observations indicated that the p50 represents the unmodified Miki and that p125 could be a post-translationally modified Miki protein, although additional experiments for confirmation are required. Also demonstrated was that siRNA#79 and #80, as well as shRNA#1 efficiently downregulate Miki expression.

To elucidate function of Miki, HeLa cells were treated with siRNAi#80 for 48 h. Mitotic cells increased from 3% (control siRNA-treated cells) to 12%, suggesting that Miki-downregulation causes mitotic arrest. As expected, Miki staining decreased significantly in cells treated with siRNA#80 (Fig. 4E, left and middle), and showed disorganized spindle formation (middle). Hoechst 33342 staining revealed scattered chromosomes (middle), which is clearly distinguishable from normal prometaphase by wide and irregular distribution of chromosomes. These abnormal prometaphases were observed in 15–43% of mitotic cells treated with either siRNA#79 or siRNA#80 (Fig. 4E, right). In contrast, cells treated with control siRNA rarely (<2%) showed scattered chromosomes. Miki-downregulation also affects nuclear morphology. Cultures of HeLa cells which stably expressed shRNA#1 frequently (approximately 20%) contained more than two nuclei (Fig. 4F, left).

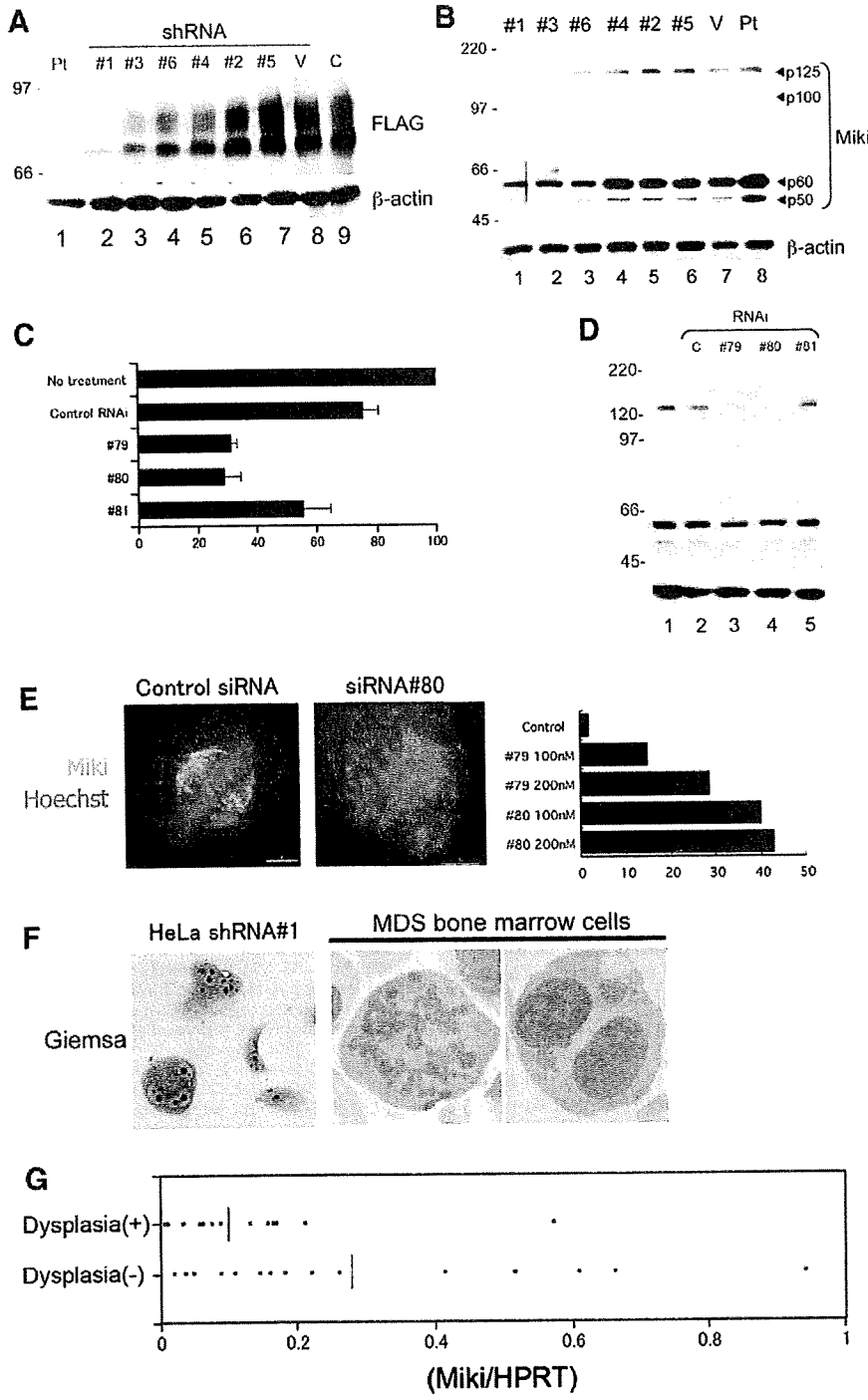


**Fig. 4.** Miki-downregulation by RNAi. (A) Immunoblot analysis using FLAG (top) or β-actin (bottom) antibodies: lane 1, lysate from untreated 293 cells; lanes 2–9, cells transfected with pcDNA3-Mikiβ-FLAG(C) with shRNA-expressing vectors for six candidate Miki-based shRNA (lanes 2–7) or empty shRNA-expressing vector (lane 8). (B) Immunoblot analysis of HeLa(tc) cells transfected with shRNA-expressing vectors for six candidate Miki-based shRNA (lanes 1–6), or an empty shRNA-expressing vector (V; lane 7). Lysates from untreated 293 cells (lane 8). (C) Miki mRNA expression levels in 293 cells treated with control siRNA, siRNA#79, #80, or #81 for 48 h are expressed as percent signal (measured using qRT-PCR) relative to an untreated control. The mean and SD for four independent experiments. (D) 293 cells were either untreated (lane 1) or transfected with control siRNA (lane 2), siRNA#79 (lanes 3), siRNA#80 (lane 4 at 40 nM), or siRNA#81 (lanes 5). (E) Immunostaining with Miki antibody of mitotic HeLa(tc) cells treated with control siRNA or siRNA#80 (48 h). DNA was stained with Hoechst 33342 (left and middle). Percentages of mitosis with scattered chromosomes in 200 mitotic cells (right). (F) Giemsa staining of HeLa cells expressing Miki shRNA#1 (left) and bone marrow cells of a MDS patient (middle and right). (G) Miki transcripts analyzed by qRT-PCR and normalized by HPRT in MDS/AML with ($n = 20$) or without ($n = 17$) dysplasia. Vertical short lines indicate average.

These findings suggested a possibility that Miki-downregulation may be implicated in mitosis with scattered chromosomes and bi- or tri-nucleated cells that are routinely observed in myeloid malignancies (Fig. 4F, middle and right). To test this hypothesis, mRNA levels of Miki in bone marrow cells from MDS or AML patients were estimated by real-time qRT-PCR. Expression levels of